



HAL
open science

Characterization of novel adsorbents from *Phoenix dactylifera* rachis. Box–Behnken design, kinetic, and isotherm models for BEZAKTIV Red S-MAX dye adsorption onto the produced carbons

Mounir Daoud, Zoubida Kecira, Oumessaâd Benturki, Pierre Girods, Yann Rogaume, Sébastien Fontana

► To cite this version:

Mounir Daoud, Zoubida Kecira, Oumessaâd Benturki, Pierre Girods, Yann Rogaume, et al.. Characterization of novel adsorbents from *Phoenix dactylifera* rachis. Box–Behnken design, kinetic, and isotherm models for BEZAKTIV Red S-MAX dye adsorption onto the produced carbons. *Biomass Conversion and Biorefinery*, 2023, 10.1007/s13399-023-04359-7 . hal-04508076

HAL Id: hal-04508076

<https://hal.science/hal-04508076>

Submitted on 19 Mar 2024

HAL is a multi-disciplinary open access archive for the deposit and dissemination of scientific research documents, whether they are published or not. The documents may come from teaching and research institutions in France or abroad, or from public or private research centers.

L'archive ouverte pluridisciplinaire **HAL**, est destinée au dépôt et à la diffusion de documents scientifiques de niveau recherche, publiés ou non, émanant des établissements d'enseignement et de recherche français ou étrangers, des laboratoires publics ou privés.

1 **Characterization of novel adsorbents from *Phoenix dactylifera* rachis. Box–**
2 **Behnken design, kinetic and isotherm models for BEZAKTIV Red S-MAX**
3 **dye adsorption onto the produced carbons**

4 Mounir Daoud ^{1,2*}, Zoubida Kecira ¹, Oumessaâd Benturki ¹, Pierre Girods ³, Yann
5 Rogaume ³, Sébastien Fontana ⁴

6 ¹ Laboratoire d'Etude Physico-chimique des Matériaux et Application à l'Environnement,
7 Faculté de Chimie, USTHB, BP 32 El-Alia, 16111, Bab Ezzouar, Alger, Algérie.

8 ² Département de Physique, Ecole Normale Supérieure Taleb Abderrahmane de Laghouat, BP
9 4033 Rue des martyrs – La gare, 03000, Laghouat, Algérie.

10 ³ Laboratoire d'Etudes et de Recherche sur le Matériau Bois, EA 4370, USC INRA,
11 Université de Lorraine, 27, rue Philippe Seguin, BP 1041, 88 051 Epinal Cedex, France.

12 ⁴ Institut Jean Lamour, UMR 7198 CNRS - Université de Lorraine 2 Allée André Guinier,
13 Campus Artem, 54000 Nancy, France.

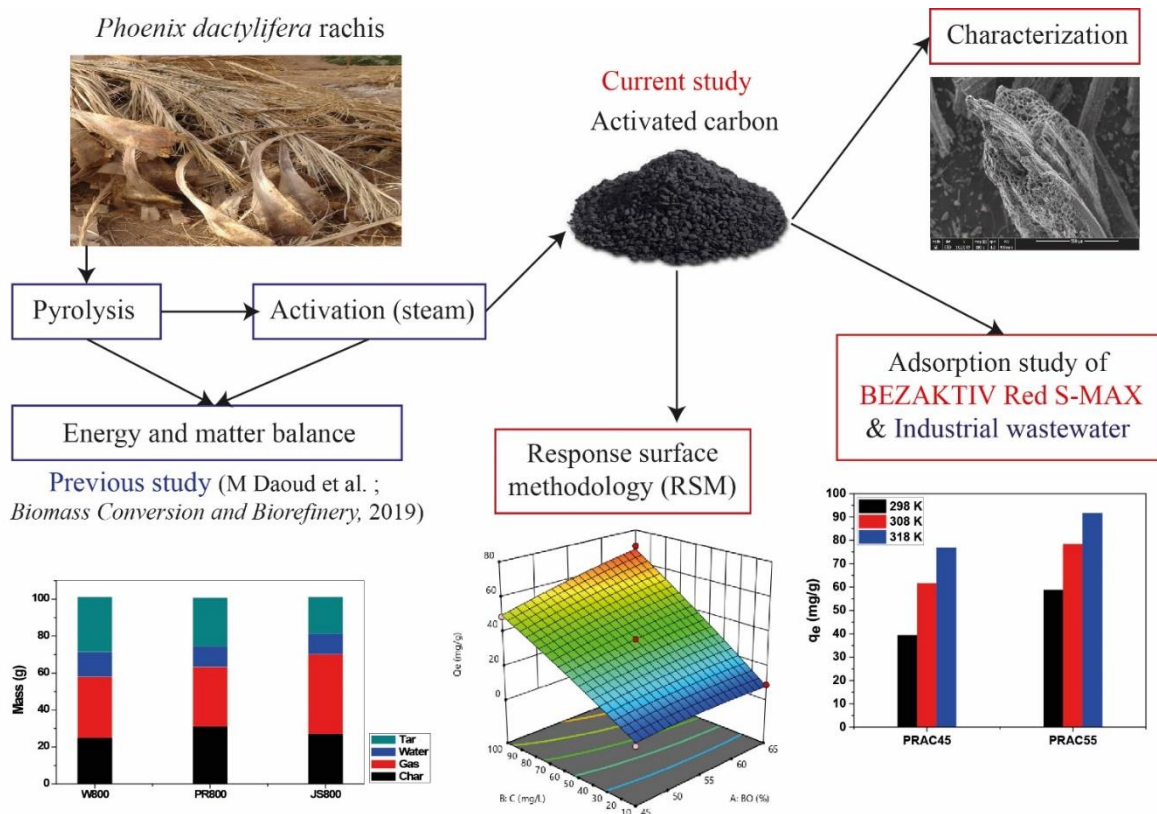
14 (*) Corresponding author e-mail: mounir.daoud@usthb.dz, da.mounir@hotmail.fr

15 **Abstract**

16 The objective of this work was to characterize the produced activated carbons based on
17 *Phoenix dactylifera* rachis (date palm rachis: **RP**) using steam with different burn-off values
18 (45, 55 and 65%), and then use those carbons to eliminate BEZAKTIV Red S-MAX (RS), a
19 commercial textile dye. The characterization of the carbons was carried out by analyzing N₂
20 adsorption-desorption, SEM, FTIR, TGA/SM, Boehm titration and pH_{PZC}. The specific
21 surface area S_{2D-NLDFT} was 500, 646 and 507 m²/g for **the activated carbons** PRAC45,
22 PRAC55 and PRAC65, respectively. The Box-Behnken design (BBD) of experiments was
23 applied to determine the influence of burn-off (A), initial concentration (B) and pH **of the**
24 solution (C) for the RS dye elimination from the aqueous system. The significant interactions
25 between the factors were AB and BC with p-value < 0.05. The RS dye adsorption
26 experiments were examined by applying the kinetic and isotherm models, and by studying
27 temperature and pH effect. It was found that the RS adsorption followed the pseudo-second-
28 order (R² > 0.99) and the removal data were well fitted to the Langmuir isotherm model. The
29 **Langmuir** maximum adsorption capacity Q_m of RS dye was 198 mg/g for PRAC55. The
30 regeneration of the carbons using thermal treatment was tested, and it revealed that the
31 specific surface area S_{2D-NLDFT} and the RS adsorption capacity Q_m increased after the
32 regeneration to 965 m²/g and 56.3 mg/g, respectively, for PRAC55. The *Phoenix dactylifera*
33 rachis adsorbents could eliminate industrial wastewater (IW) which contains BEZAKTIV
34 dyes with an adsorption rate superior to 55%.

35 **Keywords:** *Phoenix dactylifera* rachis, Adsorption, Box–Behnken design, Regeneration,
36 Dyestuff wastewater treatment

37



39

40 **1 Introduction**

41 Recently, the increase of the water source contaminated by domestic and industrial discharge
 42 is due to the development of industries and human civilization. The generated waste from this
 43 development, causes the pollution of water resources [1]. Several industries such as textile,
 44 plastic, cosmetics, agri-food, and pharmaceutical industry produce a wastewater which
 45 contains a large quantity of residual dyes [2, 3]. The textile industry is related to the word
 46 population growth that is about 8 billion which **creates** a large demand for clothing. This
 47 situation is responsible for the evolution of this industry which generates a lot of waste, in
 48 particular, wastewater. A production unit consumes approximately 1.6 million liters of water
 49 per day to produce 8,000 kg of fabric, 24% of **the** consumed water goes to the dyeing and
 50 printing sections [4]. The textile industry uses approximately 700,000 tons of dyes annually
 51 with a fixation rate on fabrics of 85 to 90%, the rest ends up in the aquatic system [5]. Most
 52 dyes and their by-products have toxic effects on the aquatic system and are harmful to the
 53 health of humans and animals such as carcinogenic and mutagenic effects [6]. The treatment
 54 of wastewater from this industry has then become a primordial necessity in producing
 55 countries.

56 Several technologies have been employed for the removal of dyes from aqueous wastewater
 57 such as photo-catalytic [7], precipitation [8], membrane filtration [9], biological method [10],
 58 ion exchange [11], and adsorption [12]. The cited methods have advantages such as removal
 59 efficiency and disadvantages such as the cost of the investment. The adsorption method is
 60 preferable among these methods for its cost, dye removal efficiency, ease of process

61 implementation [13], not generating toxic compounds, and its simplicity in the generation of
62 adsorbents [14]. To eliminate dyes from aqueous solution, various adsorbents are used such as
63 biosorbent, chitosan, clay, zeolite and activated carbon [15]. The last one i.e., activated carbon
64 is frequently used for its ability to adsorb dyes and for its physical and chemical
65 characteristics such as high surface area, porosity, thermal stability and surface chemistry
66 [16]. The cost of producing commercial activated carbons, regenerating and using them in
67 large-scale dye-contaminated water treatment operations has been raised despite their
68 mentioned characteristics; hence, we need to produce low cost and effective activated carbons
69 from inexpensive and abundant precursors [17].

70 Currently, various agricultural wastes such as apricot stones [18], argan nutshells [19], waste
71 tea [20], corncob [13], barley straw [21], and rice husk [22] have been valorized by producing
72 activated carbons. They make these wastes useful as adsorbents. Thereby, several activation
73 methods have been reported in the literature, including chemical activation using KOH [22],
74 H₃PO₄ [23] and K₂C₂O₄ [24], physical activation using CO₂ [25] and steam [20], and the
75 combined method using CO₂/CaCO₃ or K₂CO₃ [26]. *Phoenix dactylifera* rachis, is an
76 agricultural waste from the harvest of dates, which is found in abundance in the palm groves
77 of the Algerian desert. In the past, date palms were used as windbreaks in agricultural plots
78 inside the oasis, but currently their use is limited to firewood. The conversion of *Phoenix*
79 *dactylifera* rachis is a recovery approach which consists of producing low-cost adsorbents.
80 Several research works have been elaborated to fabricate activated carbons from date palm
81 rachis by applying chemical activation using KOH [27] and H₃PO₄ [28] while steam
82 activation is interesting because it limits the use of harmful chemicals.

83 This study is a continuation of the previous works [29, 30]. In the said study, the activated
84 carbons were produced using pyrolysis under N₂ followed by physical activation using steam.
85 Matter and energy balances were carried out during this fabrication process. The aim of the
86 current study is to apply the produced carbons based on *Phoenix dactylifera* rachis to remove
87 a BEZAKTIV Red S-MAX (RS): a commercial dye which is used by Algerian sewing thread
88 manufacturers. The chemical structure of the RS dye hasn't been mentioned by the producing
89 company (BEZEMA, Switzerland), and it considered this specification as know-how. The
90 carbons were characterized using physical and chemical methods such as adsorption-
91 desorption of N₂, scanning electron microscope (SEM), Fourier-transform infrared
92 spectroscopy (FTIR), Thermogravimetric Analyzer (TGA) under helium analysis coupled
93 with mass spectrometry (SM) and Boehm titration, pH of point of zero charges (pH_{PZC}). The
94 optimization of independent variables such as Burn-off of the activated carbons (BO%), initial
95 dye concentration (C₀), and pH solution were designed by Box–Behnken (BBD) as response
96 surface methodology (RSM). Then, the RS dye adsorption ability was examined by analyzing
97 adsorption kinetic, adsorption isotherm, temperature effect, pH effect and thermodynamic
98 parameters. The reuse of the adsorbents was also tested through thermal process in order to
99 evaluate the porosity of the carbons and the RS adsorption capacity after the thermal
100 treatment. The application of the carbons to remove real industrial wastewater was also
101 examined. Finally, the obtained results were compared with those from the *Ziziphus jujube*
102 stones study.

103 2 Experimental section

104 2.1 Adsorbents synthesis

105 The activated carbons tested in this work were prepared in the previous study [30]. Date palm
106 rachis was used as biomass to produce activated carbons by a physical process using steam
107 ($H_2O_{(g)}$) with different burn-off rates varying from 45 to 65%. First, the biomass was dried at
108 $105^\circ C$ for 24h, ground, and sifted (retained size 500-1000 μm). Then, the pyrolysis step was
109 realized by introducing the selected biomass in a controlled reactor ($800^\circ C$) to obtain gas,
110 condensable products, and char. Finally, the solid material was activated with steam by
111 introducing the amount of char in the activation-controlled reactor ($800^\circ C$) to produce
112 activated carbons. According to their burn-off, the obtained materials were named PRAC45,
113 PRAC55, and PRAC65.

114 2.2 Adsorbents characterization

115 The adsorption – desorption of N_2 at 77 K was carried out with a Micromeritics ASAP2020
116 adsorption instrument. Before the analysis, the adsorbents were outgassed for 12 h at $300^\circ C$.
117 The specific surface areas were determined using the BET (completed with the Rouquerol
118 correction) and the 2D-NLDFT models. The micropore volumes and pore size distributions
119 were calculated using the 2D-NLDFT model: this model can actually avoid overestimation of
120 the specific surface area by the BET model for microporous solids. 2D-NLDFT calculations
121 were realized using the software SAIEUS, with a corrugation parameter $\lambda = 4.25$ and an
122 integration range from 0.4 nm to 29.3 nm.

123 The activated carbons' surface morphology was analyzed using a scanning electron
124 microscope analyzer (Quanta FEG 120 650 electron microscope). **The electron acceleration**
125 **voltage is fixed at 10 kV. The observations are performed in secondary electron mode. The**
126 **working distance is around 10 mm.**

127 The surface chemistry of the samples was determined via Fourier-transform infrared
128 spectroscopy (FTIR- 4200, Jasco). This analysis was applied to the biomass, the activated
129 carbons before and after dye adsorption, and the regenerated carbons.

130 The activated carbons' surface functions were determined using TGA analysis (Evolution
131 1750 Setaram® thermobalance) under Helium gas coupled with mass spectrometry (Pfeiffer®
132 GSD 301C Vacuum Omnistar). The oxygenated functions present on the surface of the
133 carbons degrade during TGA measurements by releasing in a range of temperatures: CO_2 (100
134 – $650^\circ C$) and CO (350 – $1000^\circ C$) [31, 32], based on the chemical nature of the function.

135 The activated carbons' surface functions have been quantified using the Boehm titration
136 method [33]. According to the protocol, $NaOH$ (0.05 N) neutralizes phenolic, carboxyl, and
137 lactone groups (acidic groups); Na_2CO_3 (0.05 N) neutralizes carboxyl and lactone groups;
138 $NaHCO_3$ (0.05 N) neutralizes only carboxyl groups; **whereas**, HCl (0.05 N) neutralizes the
139 basic groups.

140 The pH titration method was applied to identify the prepared samples' point of zero charges
 141 (pH_{PZC}). The experiment was carried out following the protocol [34], and the value of pH_{PZC}
 142 was estimated by intercepting the pH_{final} vs. $pH_{initial}$ curve with the $pH_{initial} = pH_{final}$ line.

143 2.3 Box-Behnken design

144 This study's design of experiments was carried out based on response surface methodology
 145 (RSM). In the literature, several experimental designs were applied to optimize various
 146 operating parameters in the adsorption study, such as Central Composite Design [35],
 147 Fractional Factorial Design [36], Taguchi [37], and Box-Behnken Design [38]. And, it was
 148 found that the latter can optimize better the adsorption models [39, 40].

149 The adsorption of BEZAKTI Red S-MAX (RS) by the prepared adsorbents based on date
 150 palm rachis and activated by steam was designed by Box-Behnken design (BBD) to optimize
 151 and evaluate three independent factors: Burn-off of the activated carbons (A), dye
 152 concentration (B), and pH solution (C). The design of the experiment contains three different
 153 levels, i.e., (-1) for the low value, (0) for the medium value, and (+1) for the high value, as
 154 summarized in Table 1.

155 **Table 1: Summary of the selected factors and their levels in BBD**

Variable	Factor	Low (-1)	Medium (0)	High (+1)
Burn-off (%)	A	45	55	65
Concentration (mg/L)	B	10	45	100
pH	C	2	6	10

156 A second-order polynomial model was performed to estimate the RS adsorption as depicted in
 157 the following equation (1).

$$Y = \beta_0 + \sum \beta_i X_i + \sum \beta_{ii} X_i^2 + \sum \sum \beta_{ij} X_i X_j \quad (1)$$

158 where, Y is the response, the experimental adsorption capacity of RS, β_0 is the model
 159 constant, β_i is the linear coefficient, β_{ii} is the quadratic coefficient, and β_{ij} is the interaction
 160 coefficient, while X_i and X_j are the independent variables (A, B, and C). The selected
 161 experimental design and the response values are regrouped in Table 2 (15 runs).

162

Table 2: The experimental data of RS adsorption capacity of the activated carbons

Run	Burn-off (%) (A)	C (mg/L) (B)	pH (C)	Q _e (mg/g) Response
1	45	10	6	6.4
2	65	10	6	9.0
3	45	100	6	49.0
4	65	100	6	70.1
5	45	55	2	24.3
6	65	55	2	31.2
7	45	55	10	34.0
8	65	55	10	39.5
9	55	10	2	6.4
10	55	100	2	50.0
11	55	10	10	8.2
12	55	100	10	63.8
13	55	55	6	36.0
14	55	55	6	37.0
15	55	55	6	35.0

164 2.4 Adsorption experiments

165 The RS dye adsorption onto Date palm rachis carbons was tested in batch mode following the
 166 cited conditions in Table 2 (A: Burn-off (%), B: Dye concentration (mg/L), and pH solution).
 167 The experimental batch was carried out in a series of test tubes containing 10 mL of dye
 168 solution in contact with 10 mg of adsorbent at 25°C. The test tubes were agitated for 24 h, and
 169 the residual dye concentration was determined using a UV-Vis spectroscopy instrument
 170 (Jasco 630). Therefore, the same protocol was adopted in the adsorption study of RS dye with
 171 different conditions of dye concentration, contact time, and solution temperature. Hence, the
 172 activated carbon's adsorption capacity Q_e (mg/g) at equilibrium and the rate RS dye uptake
 173 (Removal %) were estimated using equations (2) and (3):

$$Q_e = \frac{(C_0 - C_e)V}{W} \quad (2)$$

$$Removal \% = \frac{(C_0 - C_e)}{C_0} \times 100\% \quad (3)$$

174 where C_0 (mg/L) and C_e (mg/L) are the initial and equilibrium RS dye concentration,
175 V (mL) is volume of dye solution, and W (mg) is the weight of adsorbent.

176 2.5 Recycling experiment

177 The recycling of date palm rachis carbons was realized by using desorption and thermal
178 processes. The desorption experiment was carried out by following the protocol which
179 describing in detail in [30]. For the thermal process, a mass of spent activated carbon was
180 dried and introduced into an electrical vertical furnace under N_2 flow. After 15 min, the
181 reactor temperature rose for 10K/min until 673K was reached. Then, the temperature was kept
182 constant for 1 h followed by a cooling step up to ambient temperature. The recycled carbons
183 were analyzed by the adsorption-desorption of N_2 and FTIR methods. Then, they were applied
184 to adsorb RS dye solution (100 mg/L) in order to compare the adsorption capacity of the
185 synthesized carbons and the regenerated ones after 24 h of contact time.

186 3 Results

187 3.1 Textural properties analysis

188 The textural properties of the activated carbons PRAC45, PRAC55, and PRAC65 were
189 evaluated from nitrogen adsorption-desorption isotherm at 77 K (Figure 1 (a), (b) and (c))
190 using a Micromeritics ASAP 2020. The obtained results of the collected data are regrouped in
191 Table 3. As can be observed in Figure 1 (a), (b) and (c), all the carbon's adsorption-desorption
192 isotherms rise significantly at low relative pressure indicating the microporous character of
193 the samples. Moreover, the knee of the N_2 isotherm becomes gradually more open from the
194 relative pressure P/P_0 of 0.5 and forms a hysteresis loop which indicates the development of
195 the mesoporosity by capillary condensation. The samples show a variation between types I, II,
196 and IV. Type I characterizes the microporous adsorbents [41] in the relative pressure range
197 values from 0 to 0.42 while, the presence of hysteresis loop during the desorption stage can be
198 related to the mesoporous texture. Types II and IV can be assigned to the porosity of the
199 examined biomass. Gonzalez et al. [42] have observed that the use of steam as an activating
200 agent with burn-off superior to 50% converts micropores to mesopores. The textural
201 properties of the carbons (Table 3) were determined by the BET surface model and 2D-
202 NLDFT heterogenous surface model [43] analyzing the obtained data by SAIEUS software.
203 From Table 3, the $S_{2D-NLDFT}$ was 500, 646, and 507 m^2/g for PRAC45, PRAC55, and
204 PRAC65, respectively. As can be seen, the S_{BET} rises with the increase of the burn-off rate
205 until reaching 646 m^2/g (burn-off = 55%); then, it decreases slightly until 507 m^2/g for burn-
206 off value of 65%. This could be explained by the fact that the increase in the burn-off rate
207 leads to the porous structure's formation rate that exceeds that of destruction generated from
208 the pore enlargement [44]. Thereafter, the pore enlargement becomes a dominant effect after a
209 long period of gasification by steam while pore deepening and new pore formation become
210 minor activities [41]. Hence, the increase in burn-off value affects the porosity of the
211 adsorbent by producing more mesopores. The total pore volume and micropore volume were
212 analyzed using the 2D-NLDFT model. The obtained results revealed that the total volume
213 increased from 0.383 to 0.522 cm^3/g and the micropore volume decreased from 50 to 33%,

214 with an increase in the burn-off rate from 45 to 65%. This can be explained by the fact that
 215 the augmentation in activation duration (i.e., burn-off rate) causes the enlargement of
 216 micropores resulting from the destruction of the walls between the adjacent pores [44]. The
 217 pore size distribution was evaluated by analyzing the N₂ isotherm using the 2D-NLDFT
 218 model (Figure 1 (d)). As can be noted, the pores of the examined samples are primarily
 219 located in the range of micropore (pore size < 2 nm); however, the rate of mesopore volume
 220 rises with the increase of the burn-off rate. Ruey-Shin and Al [45] observed this phenomenon
 221 in the physical activation of bagasse by using CO₂.

222 **Table 3: Textural properties of the synthesized materials PRAC45 and PRAC55.**

Textural properties	PRAC45	PRAC55	PRAC65
BET surface area (m ² /g)	583	629	608
2D-NLDFT surface area (m ² /g)	500	646	507
Total pore volume (cm ³ /g)	0.383	0.486	0.522
Micropore volume [d < 2 nm] (cm ³ /g)	0.192	0.204	0.170
Mesopore volume [d > 2 nm] (%)	50	58	67

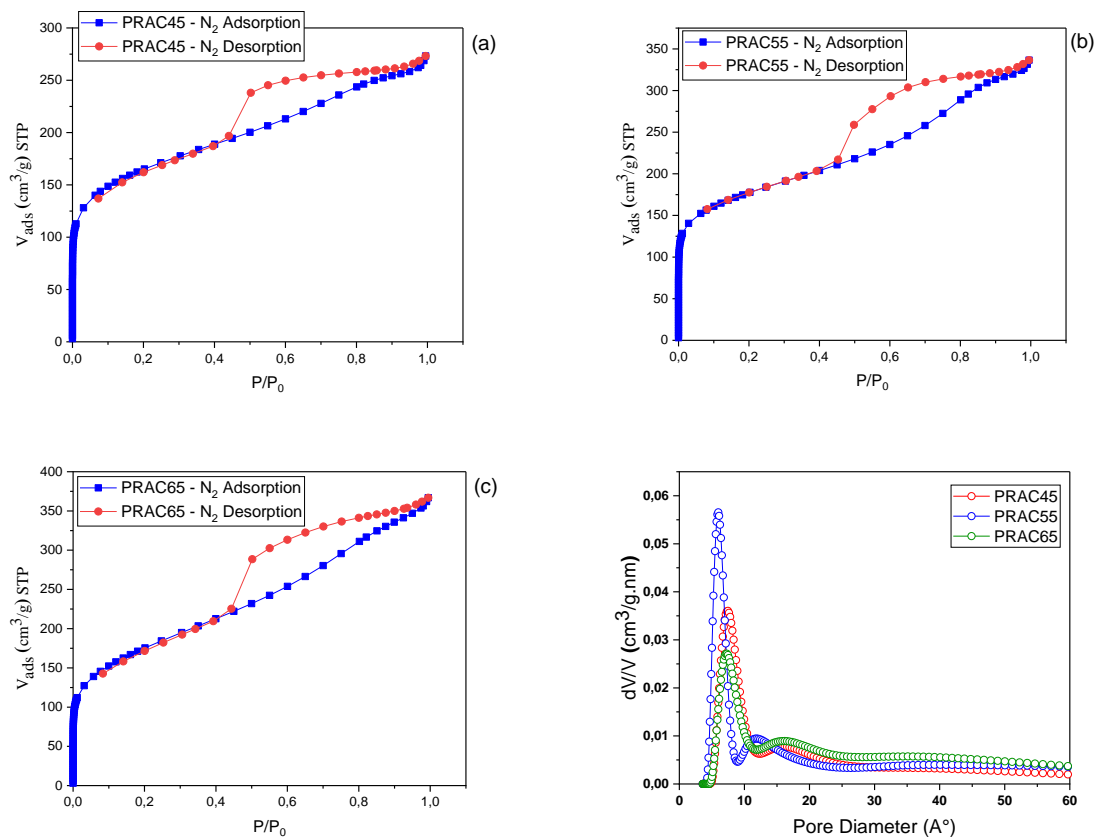


Figure 1 : (a), (b) and (c) N₂ Adsorption-desorption isotherms of PRAC45, PRAC55 and PRAC65, (d) Adsorbent's pore diameter distribution.

223 3.2 Surface properties

224 The PRAC45 and PRAC55 were selected to evaluate the influence of the burn-off rate on
225 different parameters. The visualization of sample surface morphologies has been realized
226 using SEM, as depicted in Figure 2, revealing some information regarding activated carbons
227 pore shape. Thereby, a skeleton remaining from the biomass after the steam activation process
228 is observed from Figure 2.

229

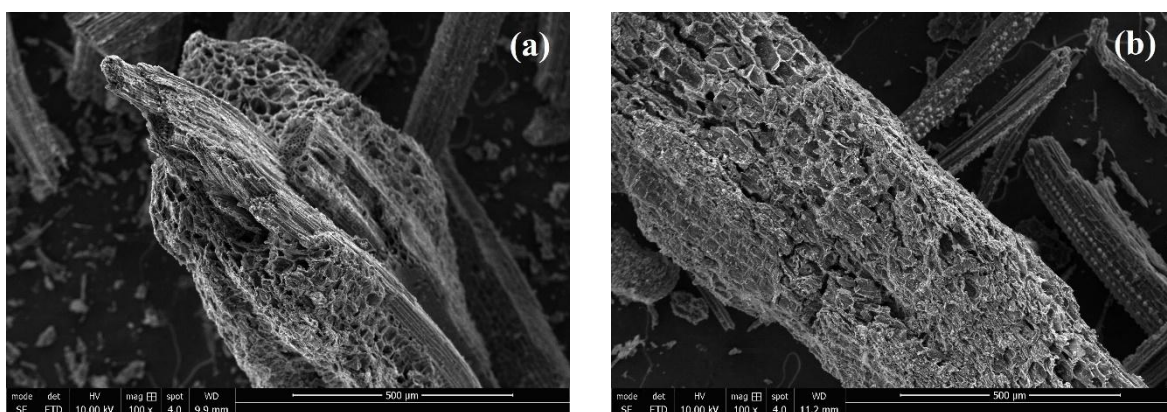
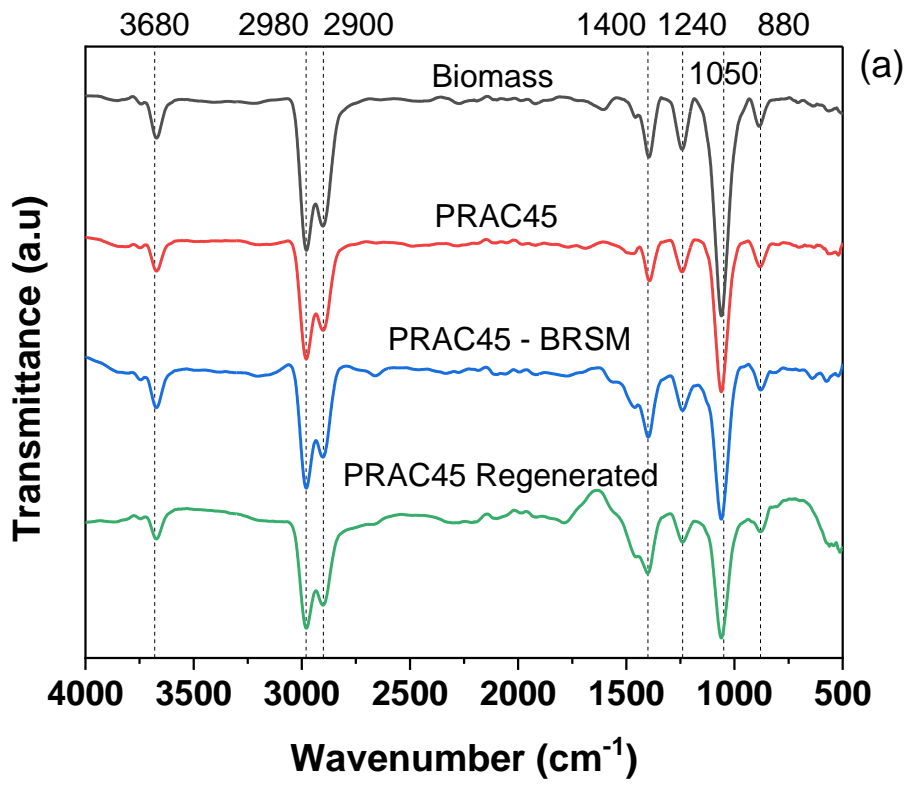
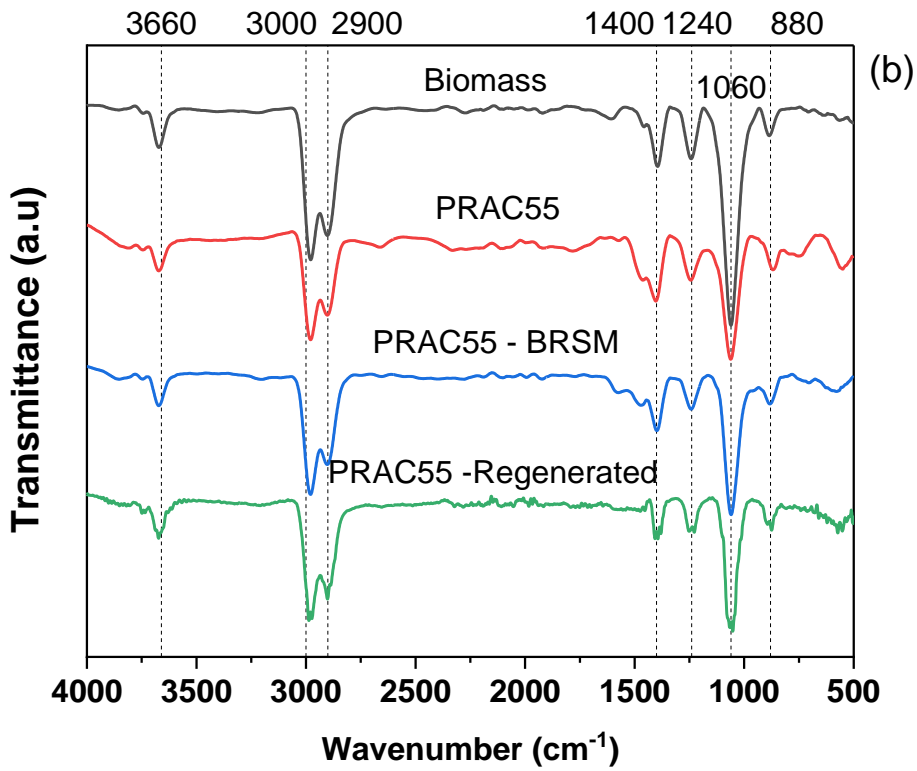


Figure 2 : The SEM images of PRAC45 (a) and PRAC55 (b).

230 The FTIR spectra of biomass (*Phoenix dactylifera* rachis), PRAC45, and PRAC55 before and
231 after RS dye contact and their regenerated carbons are presented in Figure 3. The band of
232 3660 cm^{-1} can be assigned to O–H stretching vibrations of the hydroxyl group (alcohol,
233 phenol, and absorbed water) [21]. The peaks in the range of $3000\text{--}2900\text{ cm}^{-1}$ are attributed to
234 the C–H stretching vibration of aliphatic groups [46]. The observed peaks at 1400 cm^{-1} can be
235 related to the methyl and aromatic vibrations of the sp^2 carbon (C=C). The peaks at 1240 cm^{-1}
236 correspond to the -C–OH stretching vibration; whereas, the broad peaks at 1060 cm^{-1} are
237 related to C–O–C bending vibrations. Thus, the peaks reported at 880 cm^{-1} could be assigned
238 to the aromatic out of plane C–H bending [47, 48]. The thermal treatment of the biomass using
239 pyrolysis - gasification process, and the regeneration process of the used carbons have not a
240 significant impact on the surface chemistry of the materials. This behavior was noted also in
241 the derived carbons from *Ziziphus jujube* stones [30]. However, a decrease in the intensity of
242 the peaks in the FTIR analysis was observed in the spectra of the carbons.



243

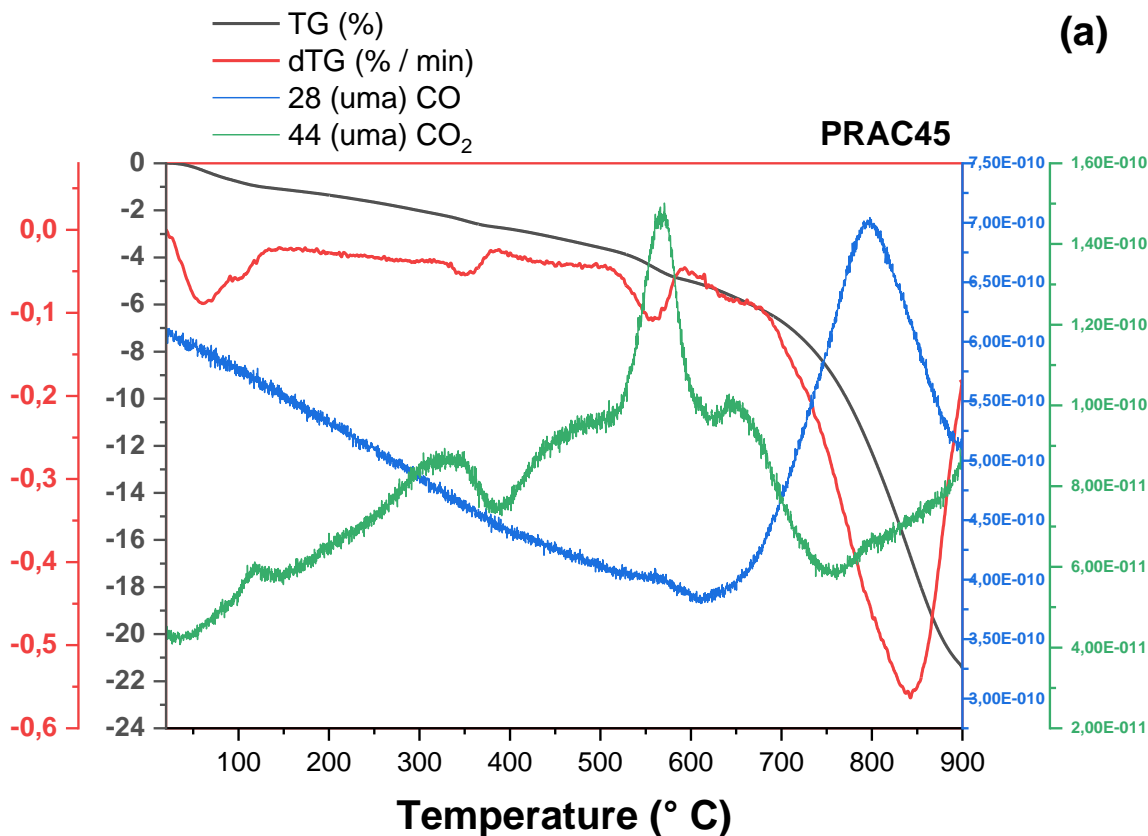


244

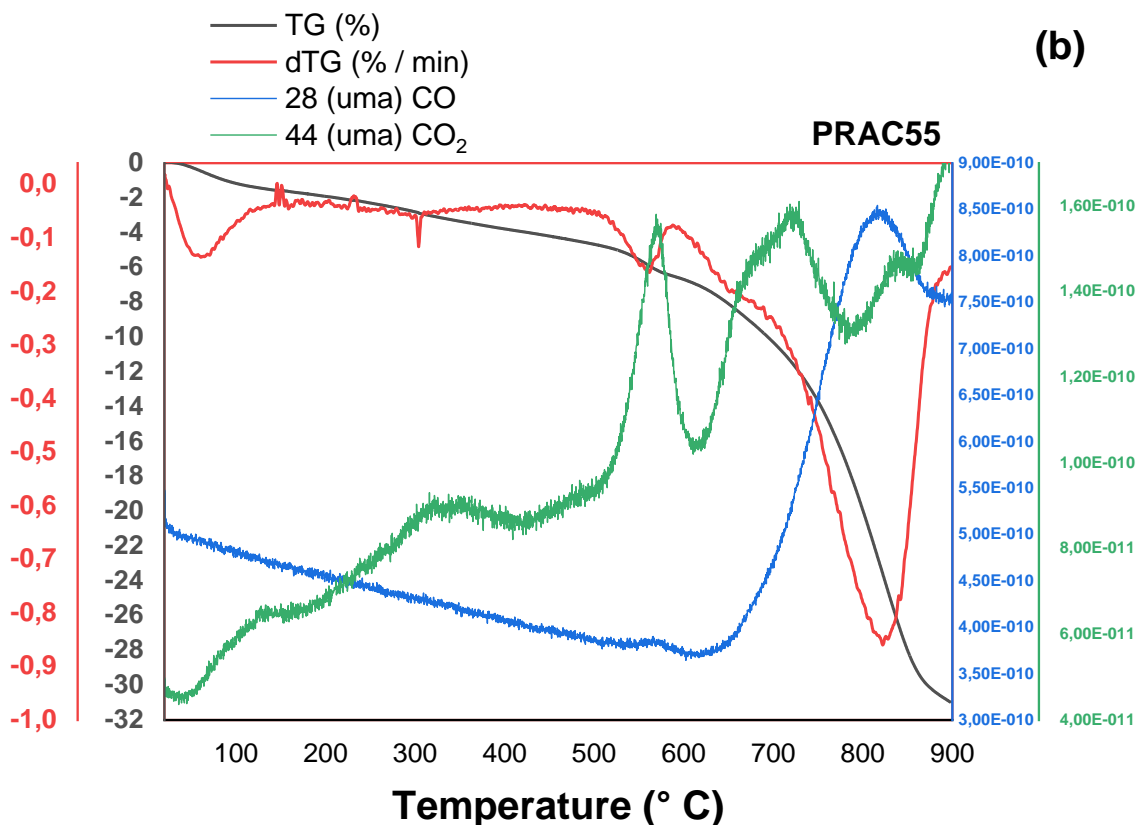
245

Figure 3: The FTIR spectra of PRAC45 (a) and PRAC55 (b).

246 The result of the coupled technique of thermogravimetric analysis and mass spectrometry
 247 TGA/SM were illustrated in Figure 4. Each material's graphical representation contains TGA,
 248 dTG, and mass spectrometry of CO (m/Z=28 uma) and CO₂ (m/Z=44 uma) spectra. As can be
 249 seen, a loss of mass of 0.8% and 1.2% for PRAC45 and PRAC55, respectively, has been
 250 observed at region of 100°C. This could be assigned to the adsorbed water on the samples'
 251 surface. The subsequent mass loss i.e. from 200°C to 800°C could be attributed as follows: (i)
 252 from 200°C to 350°C – the carboxyl groups could be related to the emission of carbon
 253 monoxide CO ; (ii) from 350°C to 800°C – also the carboxyl groups could be assigned to the
 254 emission of carbon dioxide CO₂ [31, 32]. Thus, the increase of the loss of mass of PRAC45
 255 (21.4%) and PRAC55 (30.9%) was observed with the increase of the burn-off rate (%).
 256 Moreover, the decomposition temperatures were above 500°C, which confirms that there
 257 were mainly basic functions. The observed CO peak around 800°C is certainly attributed to
 258 these basic functions. The materials' character was confirmed by Boehm titration study.



259



260

261

Figure 4: The TGA/SM spectra of PRAC45 (a) and PRAC55 (b).

262 Surface oxygen groups and measurement of surface pH were calculated in order to obtain
 263 quantitative information about the functional groups present on the adsorbents' surface. The
 264 results were summarized in Table 4. The pH_{PZC} value of PRAC45 and PRAC55 were 11.3 and
 265 11.5, respectively, showing the basic character of the materials. The gasification using H_2O
 266 produces basic adsorbents. Y.J Zhang et al. [41] has obtained similar results with the
 267 activation of bamboo chips by steam ($pH_{PZC} = 9.97 \pm 0.03$). These results are consolidated by
 268 the Boehm titration study. Consequently, the acidic and basic groups of PRAC45 and
 269 PRAC55 were presented in detail in Table 4. The contents of basic groups were greater than
 270 that of acidic groups (carboxyl, lactonic and phenolic) indicating that the physical activation
 271 using steam led to basic adsorbents. Furthermore, the more burn-off value is, the more the
 272 content of basic and acidic groups is.

273

Table 4: Chemical properties of the carbons surface

Chemical properties	PRAC45	PRAC55
Carboxylic groups (mmol/g)	0.250	0.025
Lactonic groups (mmol/g)	0.050	0.475
Phenolic groups (mmol/g)	0.025	0.075
Total surface acidic groups (mmol/g)	0.235	0.575
Total surface basic groups (mmol/g)	2.300	2.375
pH _{PZC}	11.3	11.5

275 3.3 BBD model analysis

276 In this study, the effect of burn-off (%) activated carbons, dye concentration (mg/L), and pH
 277 dye solution was applied at different levels for the adsorption of RS. Table 2 illustrates the
 278 obtained responses from the experiments of the parameter's effects on the removal of RS dye.
 279 The results were analyzed using the BBD response surface methodology. A quadratic
 280 polynomial model has been selected to develop the empirical relationship between Q_e (the
 281 response) and adsorption parameters. Furthermore, the analysis of variance by ANOVA test
 282 was evaluated for the significance of the regression model and the dye adsorption resulting
 283 data are regrouped in Figure 5 illustrated the comparison between the experimental and
 284 predicted models for RS adsorption capacity. From this plot, a straight line with very little
 285 difference in the actual and predicted plot was observed which indicates also a good-fitted
 286 model.

287 Table 5. The model is considered as significant in the ANOVA test result if the F-value is
 288 more than 5 and the p-value is less than 0.05 [49]. In this case, the F-value of the model is
 289 96.95 which implies that the model is significant, and the p-values are less than 0.05,
 290 indicating that the model terms are also significant. From Figure 5 illustrated the comparison
 291 between the experimental and predicted models for RS adsorption capacity. From this plot, a
 292 straight line with very little difference in the actual and predicted plot was observed which
 293 indicates also a good-fitted model.

294 Table 5, A, B, C, C², AB, and BC are significant model terms, and those with p-value > 0.05
 295 were excluded from the model. The Regression equation is given by the following equation
 296 (4):

$$\begin{aligned}
 Q_e \text{ (mg/g)} = & -35,8 + 1,228 A - 0,030 B + 2,64 C - 0,1686 C^2 \\
 & + 0,01028 AB + 0,01667 BC
 \end{aligned}
 \tag{4}$$

297 As can be seen in Figure 5 illustrated the comparison between the experimental and predicted
 298 models for RS adsorption capacity. From this plot, a straight line with very little difference in
 299 the actual and predicted plot was observed which indicates also a good-fitted model.

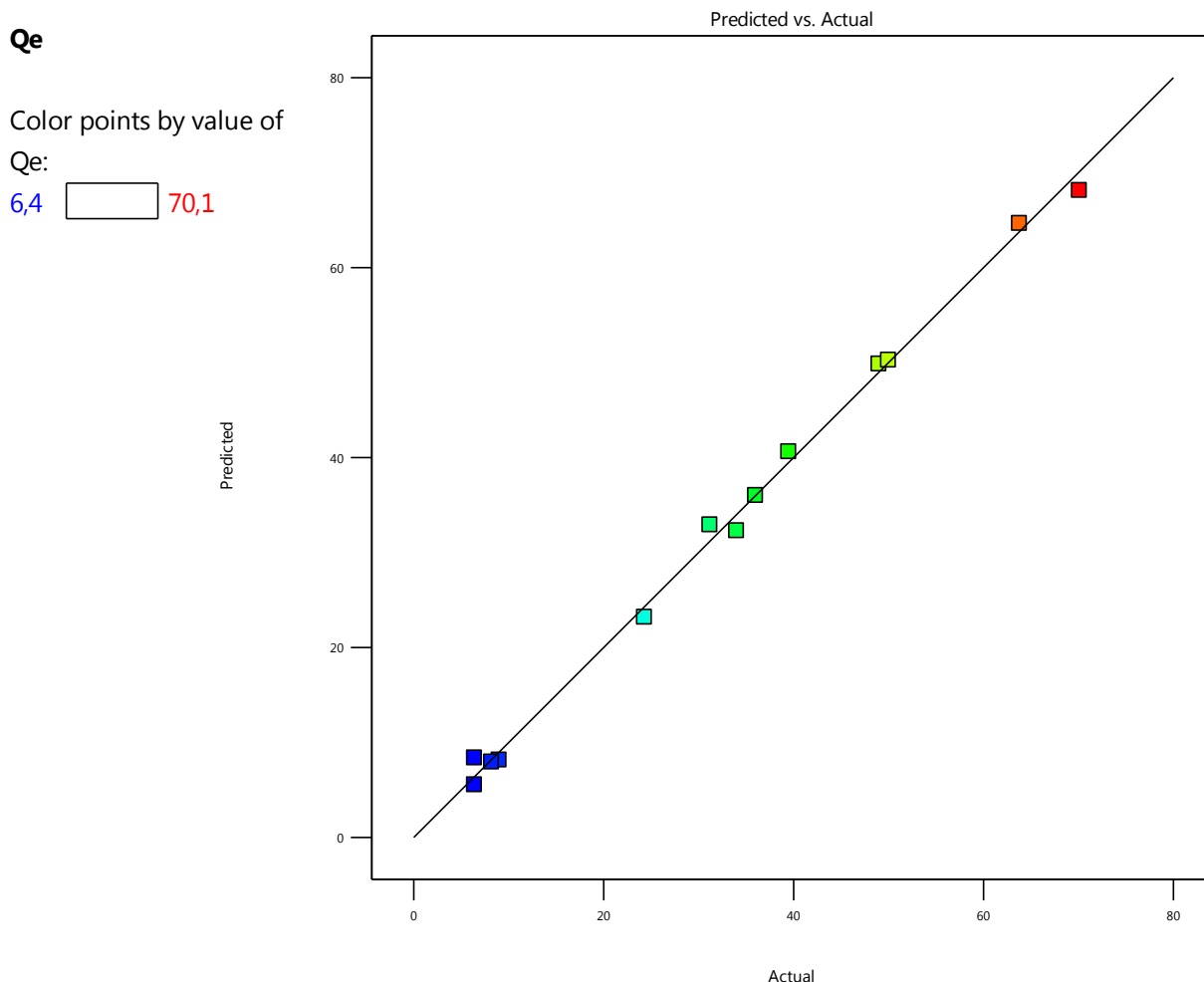
300 **Table 5**, the adjusted and predicted R² values are higher than 0.94, indicating a good
 301 correlation between predicted and experimental values. Furthermore, the Adequate Precision,
 302 which measures the signal-to-noise ratio greater than 4 (28.199), indicates that the model is
 303 desirable and the signal is adequate [50]. The reproducibility of the model is deduced from the
 304 CV% parameter, and it was found to be less than 10% (7.69%) which is considered as
 305 acceptable. Moreover, the intensity sequence of the independent variables was: B > A > C as
 306 can be deduced from the F-values [51]. Figure 5 illustrated the comparison between the
 307 experimental and predicted models for RS adsorption capacity. From this plot, a straight line
 308 with very little difference in the actual and predicted plot was observed which indicates also a
 309 good-fitted model.

310 **Table 5:** Analysis of variance (ANOVA) for the removal of RS dye.

Source	Sum of Squares	Df	Mean Square	F-value	p-value	Remark
Model	5620.07	9	624.45	96.95	< 0.001	Significant
Linear	5450.07	3	1816.69	594.23	< 0.001	
A: BO (%)	162.90	1	162.90	53.28	< 0.001	Significant
B: C (mg/L)	5146.05	1	5146.05	1683.25	< 0.001	Significant
C: pH	141.12	1	141.12	46.16	< 0.001	Significant
Square	47.95	3	15.98	5.23	0.033	
A ²	5.79	1	5.79	1.89	0.211	Insignificant
B ²	7.36	1	7.36	2.41	0.165	Insignificant
C ²	30.64	1	30.64	10.02	0.016	Significant
2-Way Interaction	122.05	3	40.68	13.31	0.003	
AB	85.56	1	85.56	27.99	0.001	Significant
AC	0.49	1	0.49	0.16	0.701	Insignificant
BC	36.00	1	36.00	11.78	0.011	Significant
Error	21.40	7	3.06			
Lack-of-Fit	19.21	3	6.40	11.71	0.019	
Pure Error	2.19	4	0.55			
Total	5641.47	16				
Std. Deviation	2.53			R ²	0.9966	
Means	32.92			Adjusted R ²	99.13	

C.V%	7.69	Predicted R ²	94.49
		Adequate Precision	28.199

311



312

313 **Figure 5:** Plot of the relationship between the predicted and actual values of RS adsorption
 314 capacity (mg/g).

315 **3.4 Effect of two parameters on RS Dye adsorption**

316 The two-way interaction between independent parameters was determined, as noted in **Figure**
 317 **5** illustrated the comparison between the experimental and predicted models for RS
 318 adsorption capacity. From this plot, a straight line with very little difference in the actual and
 319 predicted plot was observed which indicates also a good-fitted model.

320 **Table 5.** The interaction effect of the burn-off rate of the adsorbents (A) and dye
 321 concentration (B) was significant with p-value = 0.001 (**Figure 5** illustrated the comparison
 322 between the experimental and predicted models for RS adsorption capacity. From this plot, a
 323 straight line with very little difference in the actual and predicted plot was observed which
 324 indicates also a good-fitted model.

325 **Table 5**); **whereas**, the interaction between the burn-off rate of the adsorbents (A) and pH
326 solution (C) remained constant. The plots of 3-dimensional (3D) response surfaces and 2-
327 dimensional (2D) contour for the interaction and effects of burn-off rate (A) and dye
328 concentration solution (B) on RS dye adsorption capacity Q_e (mg/g) were depicted in **Figure**
329 **6** and **Figure 7**, respectively. As shown in **Figure 6** and **Figure 7**, the adsorption capacity
330 increases (from 6.4 mg/L to 70.1 mg/L) by increasing burn-off rate from 45% to 65% and the
331 dye concentration from 10 mg/L to 100 mg/L. This can be attributed to the increase of the
332 total pore volume (cm^3/g) and the mesopore volume rate % from 50% to 67% with the rise of
333 the burn-off rate % from 55% to 65%. Ruey-Shin and Al. [45] used steam to activate bagasse
334 biomass with several burn-off rates to adsorb basic dye Astrazon Red F3BL(BR22), and acid
335 dye Telon Blue ANL (AB25) found that the adsorption capacity augments with the
336 augmentation of the burn-off rate from 80.6% to 91.3%. Furthermore, it was noted from
337 **Figure 6** and **Figure 7** that the highest RS dye adsorption capacity was attained at the
338 condition of: burn-off of 65% and initial dye concentration of 100 mg/L.

339 Another significant interaction was determined between RS dye concentration (B) and pH
340 solution (C) with $p\text{-value} = 0.011$ (**Figure 5** illustrated the comparison between the
341 experimental and predicted models for RS adsorption capacity. From this plot, a straight line
342 with very little difference in the actual and predicted plot was observed which indicates also a
343 good-fitted model.

344 **Table 5**). The plots of 3-dimensional (3D) response surfaces and 2-dimensional (2D) contour
345 for the interaction and effects of dye concentration solution (B) and pH solution (C) on RS
346 dye adsorption capacity Q_e (mg/g) were showed in **Figure 8** and **Figure 9**, respectively. As
347 shown in those figures, the RS dye adsorption capacity was **augmented** by increasing the pH
348 solution until the value of 70.1 mg/g was reached in a dye concentration of 100 mg/L and pH
349 of 10. This can be interpreted by increasing the surface accessible to adsorption at basic pH.
350 Yu Kuang and Al. [52] reported similar results in the adsorption of Methylene Blue onto
351 activated carbon.

Factor Coding: Actual

Qe (mg/g)

● Design Points

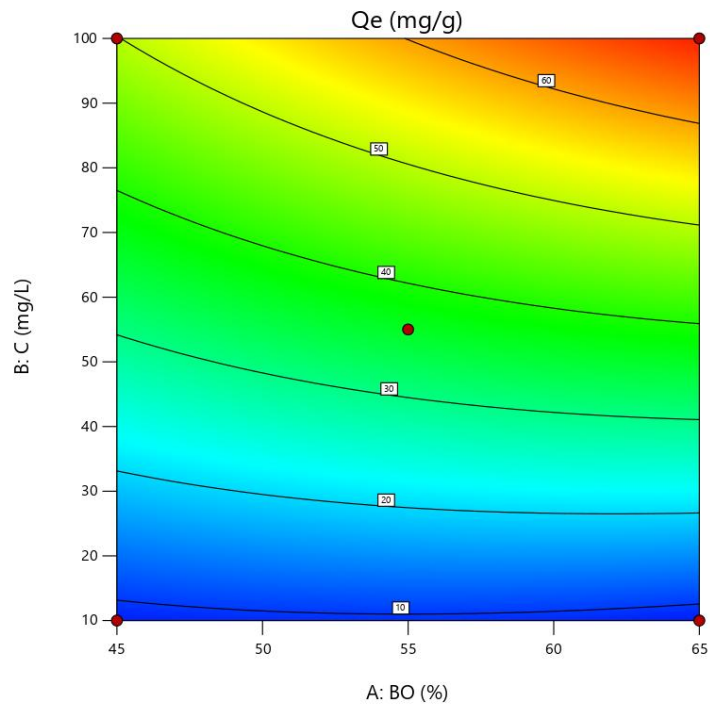
6,4  70,1

X1 = A

X2 = B

Actual Factor

C = 6



352

353 **Figure 6:** 2D contour for the interaction between burn-off rate (A) and dye concentration so-
354 lution (B).

355

Factor Coding: Actual

3D Surface

Qe (mg/g)

Design Points:

● Above Surface

○ Below Surface

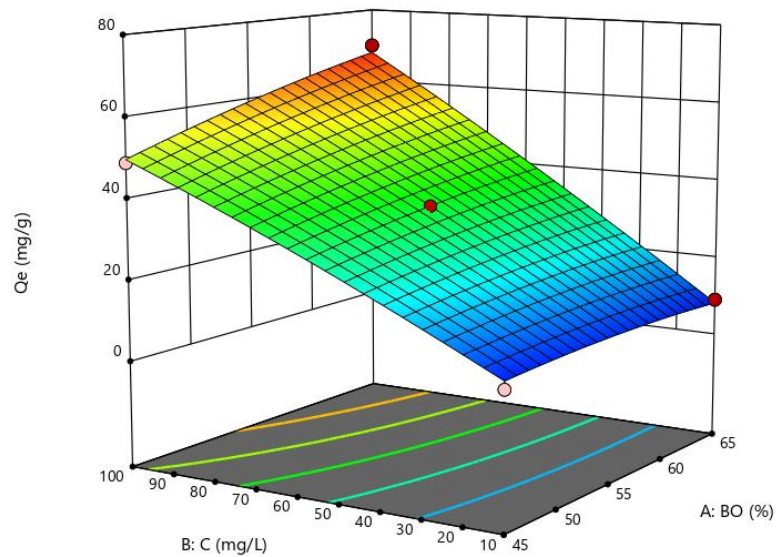
6,4  70,1

X1 = A

X2 = B

Actual Factor

C = 6

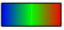


356

357 **Figure 7:** 3D response surface plot of the combined burn-off rate of adsorbents (A) and dye
358 concentration (B).

Factor Coding: Actual

Qe (mg/g)
● Design Points

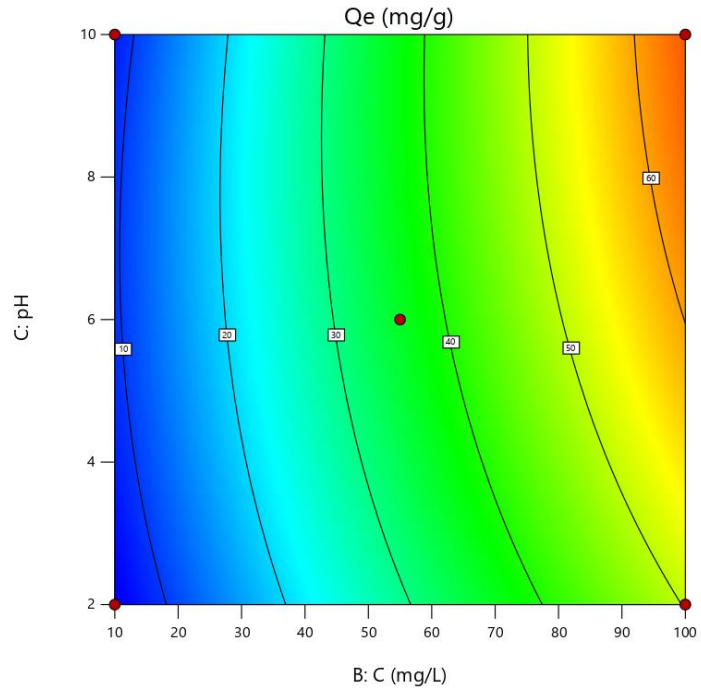
6,4  70,1

X1 = B

X2 = C

Actual Factor

A = 55



359

360 **Figure 8:** 2D contour for the interaction between RS dye concentration (B) and pH solution
361 (C).

362

Factor Coding: Actual

3D Surface

Qe (mg/g)

Design Points:

● Above Surface

○ Below Surface

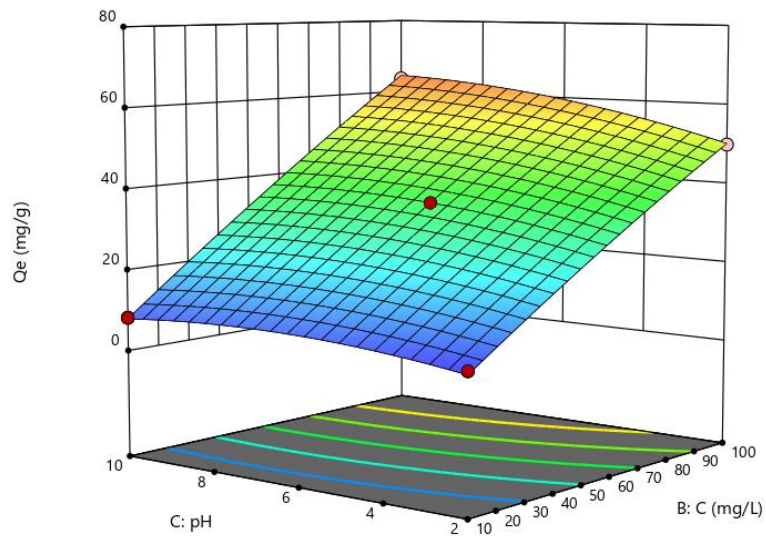
6,4  70,1

X1 = B

X2 = C

Actual Factor

A = 55



363

364 **Figure 9:** 3D response surface plot of the combined RS dye concentration (B) and pH solu-
365 tion (C).

366 3.5 Adsorption kinetic

367 The RS adsorption depends on the adsorbate concentration and time contact. A series of
368 adsorption experiments at different initial concentration of RS dye (10, 50 and 100 mg/L)
369 were carried out by varying time from 0 to 1440 min. Figure A and B (Supplementary
370 material) illustrated the RS dye removal rate (%) vs. contact time (min). As can be seen
371 clearly, both materials had the same behavior of adsorption. Thus, the removal rate decreases
372 from 82% to 55% with the augmentation of initial RS dye concentration from 10 mg/L to 100
373 mg/L using PRAC55. This could be explained by the fact that, at lower concentration, more
374 active sites in the surface of the materials were accessible for the adsorption process.
375 However, a lower adsorption rate was observed at higher concentration. This could be
376 attributed to the increase of electrostatic repulsion forces between the adsorbed RS dye
377 molecules in the material surface and RS dye in the solution [28]. Moreover, the equilibrium
378 time of the RS dye adsorption process was attained after 1440 min of contact.

379 Furthermore, the obtained data were examined by many kinetic models such as the pseudo-
380 first-order, pseudo second-order, and Elovich models, and the results were regrouped in

381 **Table 6.** The normalized standard deviation $\Delta q\%$ has been applied to determine the
382 acceptability of the employed model to explain the RS uptake process. $\Delta q\%$ is calculated
383 from the following relation (5):

$$\Delta q\% = \sqrt{\frac{1}{(N-1)} \sum_{i=1}^{i=N} \left[\frac{Q_{e,exp} - Q_{e,cal}}{Q_{e,exp}} \right]^2} \times 100\% \quad (5)$$

384 where n is the number of data points, $Q_{e,exp}$, and $Q_{e,cal}$ are the experimental and measured
385 adsorption capacities, respectively.

386 The calculated kinetic parameters are presented in

387 **Table 6.** As can be seen, for both activated carbons PRAC45 and PRAC55, the determination
388 coefficients (R^2) calculated from the pseudo second-order were close to the **unity**, and the
389 $\Delta q\%$ values were smaller than those calculated by applying **the models of** pseudo-first-order
390 **and Elovich**. This indicates that the pseudo second-order could fit well the adsorption of RS
391 dye using the examined activated carbons. In the literature, the good fit of the second-order-
392 model means that the driving force is proportional to the available fraction of **the** active sites
393 of the adsorbent, and the mechanism adsorption is a chemisorption type [53]. **The Elovich**
394 **model assumes that the activation energy rises with the evolution of the time of adsorption.**

395 Table 6 (R^2 and $\Delta q\%$) showed that this model is insufficient to describe well the RS dye
396 adsorption onto the examined carbons.

397

Table 6: Adsorption kinetic parameters of PRAC45 and PRAC55 for adsorption of RS.

C ₀ (mg L ⁻¹)	Pseudo-first order model					Pseudo-second order model				Elovich kinetic model				
	Q _{e,exp}	Q _{e,cal}	K ₁	R ²	Δq%	Q _{e,cal}	K ₂	R ²	Δq%	α	β	R ²	Δq%	
PRAC45	10	6.4	3.2	0.0113	0.979	25.4	6.8	0.0026	0.999	3.4	0.87	1.04	0.964	10.6
	50	34.1	27.2	0.0094	0.998	10.0	39.4	0.0002	0.999	7.9	0.60	0.13	0.980	10.8
	100	45.1	25.5	0.0074	0.964	21.7	46.3	0.0003	0.988	1.4	4.22	0.15	0.989	4.0
PRAC55	10	8.2	4.8	0.0166	0.973	20.5	8.8	0.0023	0.999	3.5	2.03	0.89	0.968	9.8
	50	36.1	20.7	0.0083	0.987	21.2	38.2	0.0083	0.998	3.0	2.24	0.17	0.989	5.0
	100	55.1	27.2	0.0064	0.996	25.2	55.6	0.0064	0.999	0.5	4.33	0.12	0.994	4.6

399 K₁ (1/min): the rate constant of the pseudo-first-order adsorption; K₂ (g/(mg min)): the rate constant of the pseudo-second-order adsorption ;
 400 α (mg/(g.min)): the initial adsorption rate; β (g/mg): the desorption constant.

402 The adsorption mechanism of RS dye uptake by applying PRAC45, and PRAC55 was carried
 403 out on series of steps which starts from the mobility of RS dye molecules from aqueous
 404 solution to the pores and surface of the examined materials. The aim of this step is to check if
 405 the intraparticle diffusion is the rate limiting for the adsorption of RS dye on PRAC45 and
 406 PRAC55. The Q_e (mg/g) vs. $t^{0.5}$ (min)^{0.5} was illustrated in **supplementary materials**. As can
 407 be noted, three steps were observed in this study. Firstly, a mass of RS dye molecules was
 408 transformed from the bulk solution to external surface of the carbons. Secondly, the fast step
 409 is followed by the intraparticle diffusion step which is considered as the rate limiting step.
 410 Finally, the adsorption became slow gradually until forming an equilibrium stage which
 411 means a maximum adsorption. The three parameters such as K_i , C_i and R^2 were summarized
 412 in **Table 7**. From the Table, the K_i values decrease with the increase of adsorption step
 413 progress. The thickness of the boundary layer; represented by C_i grows with the adsorption
 414 step progress which indicates a higher adsorption capacity [54]. However, the value of C_i in
 415 the second stage was non-null ($C_2 \neq 0$) for all examined tests which signifies that intraparticle
 416 diffusion was not the only rate-limiting step [55].

417 **Table 7** : Intraparticle diffusion constants of PRAC45 and PRAC55.

Intraparticle diffusion model						
$q_t = K_p t^{0.5} + C$						
	RS 10 mg/L		RS 50 mg/L		RS 100 mg/L	
	PRAC45	PRAC55	PRAC45	PRAC55	PRAC45	PRAC55
K_i (1)	0.410	0.567	1.620	2.032	2.772	3.632
C_1	0.023	0.022	0.373	0.660	0.870	0.255
R^2 (1)	0.999	0.999	0.992	0.970	0.972	0.998
K_i (2)	0.059	0.238	0.797	1.390	0.866	1.203
C_2	4.719	3.638	11.476	6.299	19.023	23.465
R^2 (2)	0.998	0.985	0.973	0.995	0.986	0.995
K_i (3)	0.009	0.023	0.128	0.275	0.209	0.518
C_3	6.059	7.408	29.110	26.024	37.045	35.882
R^2 (3)	0.999	0.759	0.999	0.915	0.999	0.961

418 K_i (mg/g min^{0.5}): the intraparticle diffusion rate constant; C: the thickness of the boundary
 419 layer.

420

421 3.6 Adsorption isotherm

422 In this work, five widely applied isotherm models (Langmuir, Freundlich, Temkin, **Sips and**
423 **Redlich–Peterson**) were analyzed in order to fit the equilibrium of the collected experimental
424 data. The objective of this part is to obtain information about the type of solute-surface
425 interaction and the effect of the adsorbate concentration on the adsorbent surface at a given
426 temperature.

427 The Langmuir adsorption isotherm was applied to determine the maximum adsorption
428 capacity (Q_{\max}). This model assumes that the adsorption of RS dye on the surface of the
429 activated carbon is a monolayer type [56]. Moreover, the dimensionless separation factor (R_L)
430 is calculated from the following equation (6):

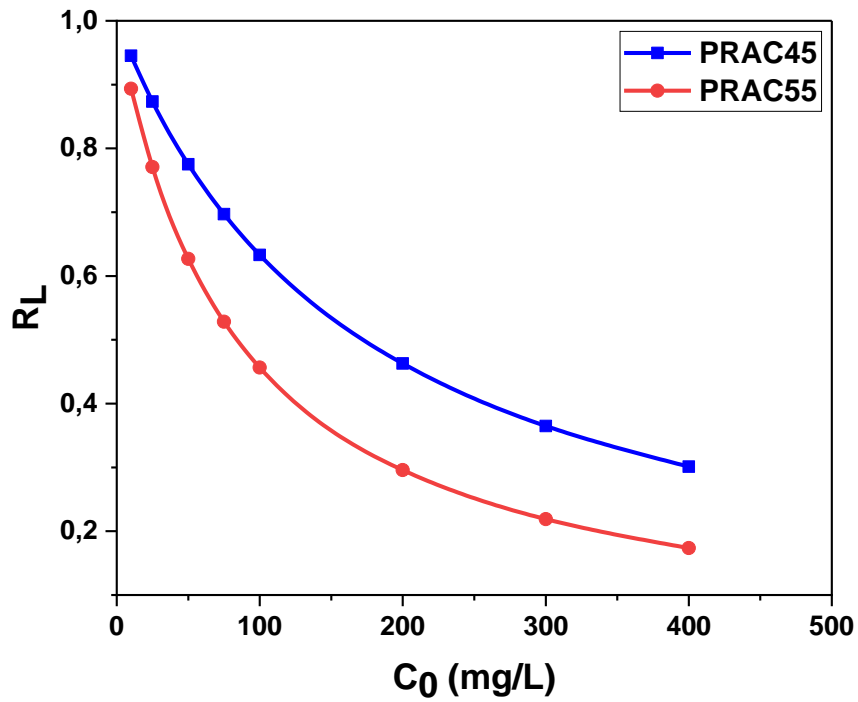
$$R_L = \frac{1}{1 + K_L C_0} \quad (6)$$

431 where K_L is the Langmuir isotherm constant and C_0 is the initial adsorbate concentration. The
432 R_L value reveals the nature of the adsorption either: irreversible ($R_L = 0$), favorable ($0 < R_L <$
433 1), linear ($R_L = 1$), or unfavorable ($R_L > 1$) [56]. The plots of R_L vs. RS dye initial
434 concentration were presented in Figure 10. As can be seen, the R_L values for the elimination
435 of RS dye by PRAC45 and PRAC55 were less than the unity which indicates that the
436 adsorption was favorable [20]. Freundlich isotherm assumes that the adsorption of RS dye on
437 the surface of the material is a multilayer type, i.e., heterogenous surface with distribution of
438 active sites [57]. The Temkin isotherm was investigated in order to study the adsorption
439 potential of the adsorbed and adsorbent solution. This model has a factor, which studies the
440 interaction of the materials (PRAC45 and PRAC55) and the RS dye aqueous solution [58]. To
441 compare these models, two statistical parameters were estimated in order to better understand
442 the behavior of dye molecules with respect to the adsorbents; the determination coefficient
443 (R^2) and the average percentage error (APE%). R^2 can be utilized to determine the good fit
444 between the model and the obtained results while APE% can be used to compare the
445 predicted and the experimental value of maximum adsorption capacity. The APE% value was
446 obtained following equation (7):

$$APE\% = \frac{\sum_{i=1}^N \left| \frac{Q_e(\text{experimental}) - q_e(\text{predicted})}{Q_e(\text{experimental})} \right|}{N} \times 100\% \quad (7)$$

447 where N is the number of experimental data. The calculated parameters from the isotherm
448 adsorption study were summarized in Table 8. As can be observed, the adsorption data
449 obtained from date palm rachis could be fit better by the Langmuir model; $R^2 > 0.98$ when
450 compared with those obtained from Freundlich, Temkin, **Sips and Redlich–Peterson** models.
451 In addition, the Langmuir model showed lower APE% values compared also with the
452 **examined** models, indicating that the adsorption of RS dye was carried out by forming a
453 monolayer on the surface of the examined carbons [59]. The maximum adsorption capacity of
454 **Langmuir** was 169 and 198 mg/g for the adsorption of RS dye onto PRAC45 and PRAC55,
455 respectively. This may be due to the specific surface area of the cited adsorbents; $S_{2D-NLDFT} =$

456 500 and 646 m²/g for PRAC45 and PRAC55, respectively). The more the $S_{2D-NDFT}$ is, the
457 more the Q_m is. Otherwise, the maximum adsorption capacity was also estimated by Sips
458 model (3 parameters), but it was found that $APE\%_{Sips}$ superior to $APE\%_{Langmuir}$, confirming
459 that the Langmuir model describes well the RS adsorption process.



460

461 **Figure 10:** Separation factor, R_L vs. RS dye Initial concentration using PRAC45 and PRAC55
462 as adsorbents.

463

464

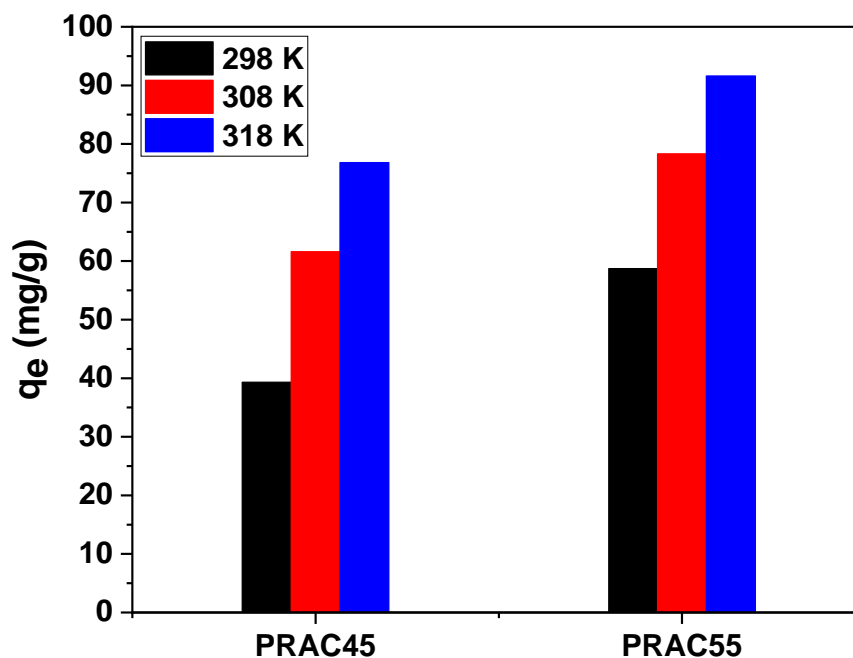
465 **Table 8:** Isotherm's parameters calculated from Langmuir, Freundlich, and Temkin models

	PRAC45	PRAC55
Langmuir	$q_e = \frac{Q_m K_L C_e}{1 + K_L C_e}$	
Q_m (mg/g) _{exp}	169	198
K_L (L/mg)	0.0058	0.0119
R^2	0.985	0.982
APE%	6.5	4.0
Freundlich	$q_e = K_F C_e^{\frac{1}{n}}$	
K_F (mg/g (L/mg) ^{1/n})	3.6	9.2
n	1.65	1.95
R^2	0.960	0.948
APE%	6.7	16.5
Temkin	$q_e = \frac{RT}{b_T} \ln(C_e K_T)$	
K_T (L/mg)	0.174	0.283
b_T (J/mg)	106.4	79.1
R^2	0.853	0.891
APE%	18.1	22.4
Sips	$q_e = \frac{Q_m K_S C_e^m}{1 + K_S C_e^m}$	
Q_m (mg/g) _{exp}	141	166
K_S (L/mg) ^m	0.0084	0.0177
m	1.192	1.332
R^2	0.976	0.986
APE%	12.4	14.3
Redlich–Peterson	$q_e = \frac{K_{RP} C_e}{1 + a_{RP} C_e^\beta}$	
K_{RP} (L/g)	0.754	1.751
a_{RP} (L/mg) ^β	4.37 10 ⁻⁵	4.09 10 ⁻⁴
β	1.792	1.546
R^2	0.981	0.985
APE%	11.8	10.2

466 q_e (mg/g): the amount of adsorbed dye; C_e (mg/L): the equilibrium concentration of dye
467 solution; Q_m (mg/g): the maximum adsorption capacity; K_L (L/mg): the Langmuir adsorption
468 constant; K_F : the adsorption capacity of the adsorbent; n : heterogeneity factor; K_T (L/mg):
469 the adsorption capacity; b_T (J/mol): Temkin constant which is related to the heat of sorption.
470 K_S (L/mg)^m is the Sips equilibrium constant; m is the dimensionless heterogeneity factor
471 ($0 \leq m \leq 1$), $m=1 \Rightarrow$ homogeneous adsorption process. K_{RP} (L/g) and β are the Redlich Peterson
472 constants, $\beta = 1 \Rightarrow$ Langmuir isotherm, $\beta \approx 0 \Rightarrow$ Freundlich isotherm.

473 3.7 Temperature effect

474 By mixing 10 mg of carbon with 10 mL of RS dye (100 mg/L), it was possible to measure the
475 impact of solution temperature on RS dye uptake. The solid/liquid system was mixed under
476 the following conditions: 24 h of contact time and pH solution of 6.3 at temperatures of 298,
477 308 and 318 K. Figure 11 illustrates the effect of the temperature on the solid/liquid system.
478 It is clear that the adsorption capacity rises from 39.3 and 58.7 mg/g to 76.8 and 91.6 mg/g
479 with the augmentation of the solution temperature from 298 to 318K for PRAC45 and
480 PRAC55, respectively. This indicates that the adsorption of RS dye onto the examined
481 materials was an endothermic process. This could be due to the increase in the mobility of the
482 RS dye molecules accompanied by a decrease in the viscosity of the solution, which generates
483 an augmentation in the molecule's rate of diffusion through the external boundary layer and
484 the internal pores of the carbon [60]. A similar trend has been mentioned in the literature [61].

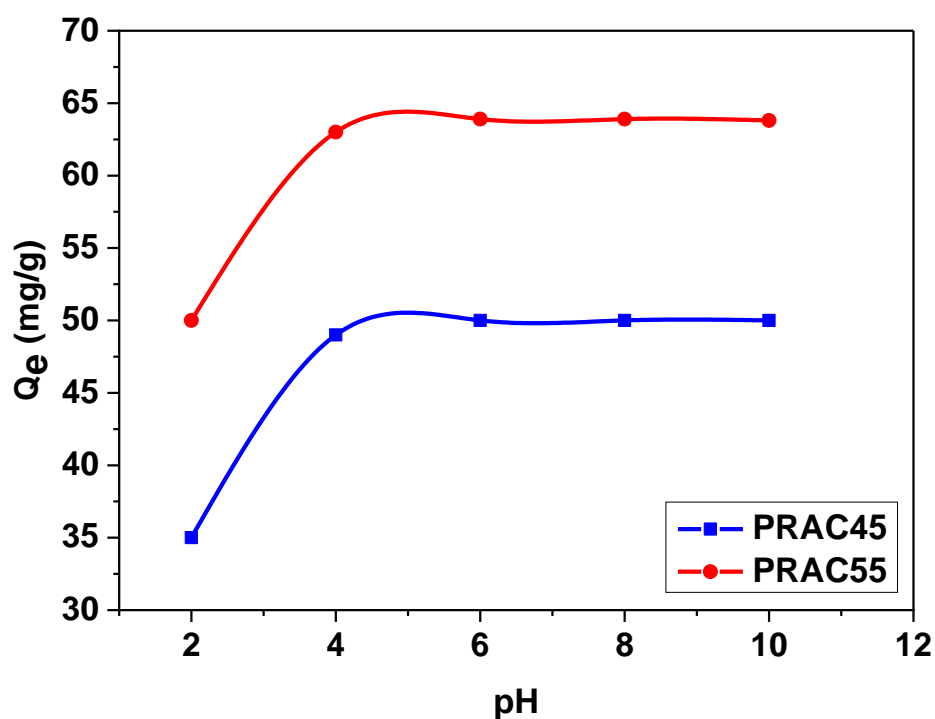


485

486 **Figure 11:** The solution temperature effect on the RS dye adsorption onto PRAC45 and
487 PRAC55.

488 **3.8 pH effect**

489 The influence of pH solution was studied in order to evaluate its impact on the elimination of
490 RS dye using PRAC45 and PRAC55. This effect was examined from pH 2 to pH 10 applying
491 the following conditions: 10 mg of carbon, 10 mL of RS dye solution and 100 mg/L of initial
492 dye concentration at 25°C. The pH solution was adjusted by using solutions of HCl and
493 NaOH 0.1 N. As shown in Figure 12, the adsorption capacity of RS dye grew from 35 and 50
494 mg/g to 50 and 63.9 mg/g (for PRAC45 and PRAC55, respectively) with the increase of pH
495 until pH 4. Then, no change is observed. The seen decrease in RS adsorption at pH 2 could be
496 attributed to the competition between RS molecules and the H⁺ ions surplus in the solution for
497 the active sites on the date palm rachis adsorbents [62]. And, the number of negative sites
498 augments with the increase of pH solution which makes the sites suitable for adsorption [63].
499 Similar behavior has been reported for the removal of methylene blue by Wishal et. al [64].



500

501

Figure 12: Effect of pH on the adsorption of RS dye.

502 **3.9 Thermodynamic study**

503 The thermodynamic study was carried out by determining the adsorption thermodynamic
504 parameters such as Gibbs free energy change (ΔG°), enthalpy change (ΔH°) and entropy
505 change (ΔS°). The said parameters were measured following the equations (8) and (9):

$$\Delta G^\circ = -RT \ln K_C \quad (8)$$

$$\Delta G^\circ = \Delta H^\circ - T\Delta S^\circ \quad (9)$$

506 Equation (8) and Equation (9) can be expressed as Equation (10):

$$\ln K_C = \frac{-\Delta H^\circ}{RT} + \frac{\Delta S^\circ}{R} \quad (10)$$

$$K_C = \frac{Q_e}{C_e} \quad (11)$$

507 Where K_C is the equilibrium constant, Q_e (mg/g) is the equilibrium concentration of RS dye
 508 on adsorbent and C_e (mg/L) is the concentration by equilibrium, T absolute temperature (K),
 509 and R is the universal gas constant (8.314 J/mol. K). The thermodynamic parameters were
 510 acquired from the plot of $\ln K_C$ vs. $1/T$, and they have been regrouped in Table 9. The
 511 negative values of ΔG° reveal that the adsorption of RS dye on the activated carbons is
 512 spontaneous; **whereas**, the positive values of ΔH° (64.34 and 80.17 kJ/mol for PRAC45 and
 513 PRAC55, respectively) indicate that the adsorption phenomenon is endothermic. Furthermore,
 514 the positive values of ΔS° show an increase in randomization or disorder [65]. **Similar**
 515 **behavior was also observed by other researchers [55].**

516 **Table 9:** The RS adsorption thermodynamic parameters of PRAC45 and PRAC55.

	ΔH° (kJ/mol)	ΔS° (J/mol)	ΔG° (kJ/mol)			R^2
			298 K	308 K	318 K	
PRAC45	64.34	212.4	-1.077	-1.210	-3.165	0.997
PRAC55	80.17	271.6	-3.286	-3.286	-6.317	0.995

517 3.10 Recycling of date palm rachis adsorbents

518 The aim of this part is to study **the RS desorption process then** the porosity and the adsorption
 519 capacity of the spent activated carbons after the thermal treatment. **For the desorption process,**
 520 **the distilled water was used as desorption medium; however, it was found that the**
 521 **desorption of RS dye was negligible after 24 h of contact time. Whereas,** several parameters
 522 **in the thermal process** were tested such as the BET surface area, 2D-NLDFT surface area,
 523 total volume pore volume, micropore volume and FTIR analysis before and after **thermal**
 524 **treatment**. The loss in material after recycling process was also tested. Table 10 summarized
 525 the obtained results. It was found that the surface area of the samples increases considerably
 526 after thermal treatment for both materials from 500 and 646 m²/g to 985 and 865 m²/g for
 527 PRAC45 and PRAC55, respectively. The pore volume was also augmented from 0.383 and
 528 0.486 cm³/g to 0.569 and 0.618 cm³/g for PRAC45 and PRAC55, respectively. This could be
 529 explained by the fact that the thermal treatment of the activated carbon generates a release of
 530 volatile matter from the sample. **This** leads to an increase in the porous structure which will
 531 be more developed than that of the activated carbon before its regeneration [21]. Moreover,

532 the adsorption capacity of RS dye increases slightly from 45.1 and 55.1 mg/g to 45.7 and 56.3
 533 mg/g for PRAC45 and PRAC55, respectively. **This is due** to the augmentation of the
 534 micropore and mesopore volume of the recycled carbons. **On the other side**, the mass loss of
 535 the material could be explained by releasing matter as gases i.e., H₂O, CO₂, CO, H₂, ... [66].
 536 The FTIR spectra of regenerated carbons are presented in [Figure 3](#). As can be seen, no
 537 significant modification of surface chemistry has been observed after the thermal treatment of
 538 the materials.

539 **Table 10:** Parameters PRAC 45 and PRAC55 regeneration

	PRAC45	PRAC55
Before recycling		
RS adsorption after 24h (mg/g)	45.1	55.1
BET surface area (m ² /g)	583	629
2D-NLDFT surface area (m ² /g)	500	646
Total pore volume (cm ³ /g)	0.383	0.486
Micropore volume (%) (d < 2 nm)	50	42
After recycling		
RS adsorption after 24h (mg/g)	45.7	56.3
Loss in material %	22	20
BET surface area (m ² /g)	883	814
2D-NLDFT surface area (m ² /g)	985	865
Total pore volume (cm ³ /g)	0.569	0.618
Micropore volume (%) (d < 2 nm)	54	44

540 **3.11 Comparative study and the adsorption of dyestuff wastewater**

541 The goal of this part is to compare RS dye adsorption ability from materials based on two
 542 biomasses; i.e., *Ziziphus jujube* stones [30] and *Phoenix dactylifera* rachis. The comparative
 543 study was carried out for the carbons that are activated only by steam and under the same
 544 conditions (burn-off rate, pyrolysis and activation parameters). Thus, different factors have
 545 been examined, including specific surface area (S_{2D-NLDFT}), RS dye maximum adsorption
 546 capacity Q_m (mg/g), total pore volume (cm³/g), micropore volume (%), and total surface of
 547 acidic and basic groups (mmol/g). [Table 11](#) summarized the obtained results. As can be
 548 observed, the *Ziziphus jujube* stones carbons possess the higher values of the specific surface
 549 area, total pore volume and micropore volume, **but they** present the lowest values of the
 550 maximum adsorption capacity Q_m. **On the other hand**, the *Phoenix dactylifera* carbons adsorb

551 better the RS dye ($Q_m = 198$ mg/g for PRAC55) while they have specific surface areas lower
 552 than that of the *Ziziphus jujube* stones carbons. This could be related to the number of the
 553 basic groups of the *Phoenix dactylifera* carbons which were superior to those of *Ziziphus*
 554 *jujube* stones carbons.

555 Furthermore, the adsorption of real dyestuff wastewater which contains RS dye and other
 556 range dyes of BEZAKTIV was examined in this comparative study. The solution was
 557 collected from the industrial dye bath after the sewing thread dyeing process, while the
 558 dyestuff wastewater treatment was described in detail in [30]. The percentage of industrial
 559 wastewater removal (IW%) obtained from the utilization of the examined activated carbons
 560 (after 48h of contact time) was used as comparative parameters, and the results were
 561 illustrated in Table 11. As can be seen, the *Phoenix dactylifera* rachis carbons eliminated
 562 better the real wastewater than the *Ziziphus jujube* stones ones. The IW% reached 55.2% and
 563 68.2% using PRAC45 and PRAC55, respectively, which could be explained by the high
 564 number of basic groups of the *Phoenix dactylifera* rachis materials. This result is in agreement
 565 with the RS adsorption study.

566 **Table 11:** Comparative study between the *Ziziphus jujube* stones and *Phoenix dactylifera*
 567 rachis activated using steam.

	JSAC45 [30]	JSAC55 [30]	PRAC45	PRAC55
$S_{2D-NLDFT}$ (m ² /g)	1095	1075	500	646
Q_m (mg/g)	106.1	113.3	169.0	198.0
IW% (after 48h of contact time)	39.3	41.8	55.2	68.2
Pore volume (cm ³ /g)	0.489	0.471	0.383	0.486
Micropore volume (%)	72.6	76.2	50.0	42.0
Total surface acidic groups (m mol/g)	0.275	0.450	0.235	0.575
Total surface basic groups (m mol/g)	0.725	0.925	2.300	2.375
Total surface groups (mmol/g)	1.000	1.375	2.535	2.950

568 4 Conclusion

569 In the present work, the date palm rachis carbons were characterized by physicochemical
 570 methods. The obtained results indicated that the $S_{2D-NLDFT}$ was 500, 646 and 507 m²/g for
 571 PRAC45, PRAC55 and PRAC65, respectively. Boehm titration and pH_{PZC} showed that the
 572 carbons have a basic character. Response surface methodology by the Box–Behnken model
 573 was employed to examine the role and effect of three parameters .i.e. carbon burn-off (%),
 574 initial RS dye concentration (mg/L), and pH solution for BEZAKTIV Red S-MAX removal.
 575 The results showed significant interactions between AB (carbons burn-off x initial RS dye
 576 concentration, p-value = 0.001), and BC (initial RS dye concentration x pH solution, p-value
 577 = 0.011). The kinetic and isotherm adsorption were investigated, revealing the very good fit
 578 of the pseudo-second-order equation, and Langmuir models. The maximum RS dye

579 adsorption capacity was found 198 mg/g by using PRAC55. The thermodynamic study
580 **revealed** that the adsorption process was endothermic. The recycling of the spent activated
581 carbons was carried out using thermal treatment. It was found that the regeneration process
582 increases the specific surface area ($S_{2D-NLDFT}$) of the carbons (**PRAC45: from 500 to 985**
583 **m²/g**). The carbons were also applied to eliminate industrial wastewater, and the adsorption
584 rate (IW%) was 55.2% and 68.2% using PRAC45 and PRAC55, respectively. Therefore, the
585 *Phoenix dactylifera* materials could be classified as effective adsorbents for the removal of
586 Red S-MAX dye.

587 **Acknowledgements**

588 The authors would like to thank Matthieu DEBAL for his assistance in the biomass
589 conversion process and Zineb THAMINY for her assistance in the English language. They
590 would also like to thank Omar BENKIH for providing Reactive dye.

591 Declaration of interest statement

592 There is no conflict interest that could have appeared to influence the work reported in this
593 paper.

594 **Author contribution statements**

595 Mounir Daoud designed and performed the experiments, derived the models, and interpreted
596 the results. Oumessaâd Benturki and Yann Rogaume supervised the project and were in
597 charge of the overall direction. Zoubida Kecira assisted with FTIR measurements and helped
598 carry out the dye adsorption study. Sébastien Fontana characterized the adsorbents with
599 several methods (N₂ Adsorption, TGA/SM, and SEM). Pierre Girods supervised the
600 production of the adsorbents and analyzed them with Elemental analysis. Mounir Daoud
601 analyzed the data and wrote the manuscript in consultation with Sébastien Fontana and Pierre
602 Girods. The authors have read and agreed the published version of the manuscript.

603 **Funding**

604 The work was financially supported by the Ecole Normale Supérieure Taleb Abderrahmane of
605 Laghouat (Algeria), the Laboratory for Physico-chemical Study of Materials and Application
606 on the Environment, Faculty of Chemistry, USTHB, Algiers (Algeria), and the University of
607 Lorraine (France).

608 **Data availability and materials:** Not applicable.

609 **Declarations**

610 **Ethical approval:** Not applicable.

611 **Conflict of interest:** The authors declare no competing interests.

612 **5 References**

- 613 1. Hamidi F, Dehghani MH, Kasraee M, et al (2022) Acid red 18 removal from aqueous solution
614 by nanocrystalline granular ferric hydroxide (GFH); optimization by response surface
615 methodology & genetic-algorithm. *Sci Rep* 12:1–15
- 616 2. Acisli O, Khataee A, Karaca S, Sheydaei M (2016) Modification of nanosized natural
617 montmorillonite for ultrasound-enhanced adsorption of Acid Red 17. *Ultrason Sonochem*
618 31:116–121
- 619 3. Ashrafi SD, Rezaei S, Forootanfar H, et al (2013) The enzymatic decolorization and
620 detoxification of synthetic dyes by the laccase from a soil-isolated ascomycete,
621 *Paraconiothyrium variabile*. *Int Biodeterior Biodegradation* 85:173–181
- 622 4. Kant R (2012) Textile dyeing industry an environmental hazard. *J Nat Sci* 4 (1): 22–26
- 623 5. Moyo S, Makhanya BP, Zwane PE (2022) Use of bacterial isolates in the treatment of textile
624 dye wastewater: A review. *Heliyon* e09632
- 625 6. Tony BD, Goyal D, Khanna S (2009) Decolorization of textile azo dyes by aerobic bacterial
626 consortium. *Int Biodeterior Biodegradation* 63:462–469
- 627 7. Haghghi M, Rahmani F, Dehghani R, et al (2016) Photo-catalytic activity of ZnO supported on
628 H-ZSM-5 zeolite to reduce Cr (VI) from aqueous solutions. *Int Arch Heal Sci* 3:1–6
- 629 8. Stylianou S, Simeonidis K, Mitrakas M, et al (2018) Reductive precipitation and removal of Cr
630 (VI) from groundwaters by pipe flocculation-microfiltration. *Environ Sci Pollut Res* 25:12256–
631 12262
- 632 9. Mukherjee R, Bhunia P, De S (2019) Long term filtration modelling and scaling up of mixed
633 matrix ultrafiltration hollow fiber membrane: a case study of chromium (VI) removal. *J Memb*
634 *Sci* 570:204–214
- 635 10. Barbosa PFP, Cumba LR, Andrade RDA, do Carmo DR (2019) Chemical modifications of
636 cyclodextrin and chitosan for biological and environmental applications: metals and organic
637 pollutants adsorption and removal. *J Polym Environ* 27:1352–1366
- 638 11. Homan NP, Green PG, Young TM (2018) Evaluating ferrous chloride for removal of chromium
639 from ion-exchange waste brines. *Journal-American Water Work Assoc* 110:E43–E54
- 640 12. Vilela PB, Dalalibera A, Duminelli EC, et al (2019) Adsorption and removal of chromium (VI)
641 contained in aqueous solutions using a chitosan-based hydrogel. *Environ Sci Pollut Res*
642 26:28481–28489
- 643 13. Li H, Gao P, Cui J, et al (2018) Preparation and Cr (VI) removal performance of corncob
644 activated carbon. *Environ Sci Pollut Res* 25:20743–20755
- 645 14. Ren L, Xu J, Zhang Y, et al (2019) Preparation and characterization of porous chitosan
646 microspheres and adsorption performance for hexavalent chromium. *Int J Biol Macromol*
647 135:898–906
- 648 15. Borna MO, Pirsaeheb M, Niri MV, et al (2016) Batch and column studies for the adsorption of
649 chromium (VI) on low-cost *Hibiscus Cannabinus* kenaf, a green adsorbent. *J Taiwan Inst Chem*
650 *Eng* 68:80–89

- 651 16. Seidmohammadi A, Asgari G, Dargahi A, et al (2019) A comparative study for the removal of
652 methylene blue dye from aqueous solution by novel activated carbon based adsorbents. *Prog*
653 *Color Color Coatings* 12:133–144
- 654 17. Cazetta AL, Vargas AMM, Nogami EM, et al (2011) NaOH-activated carbon of high surface area
655 produced from coconut shell: Kinetics and equilibrium studies from the methylene blue
656 adsorption. *Chem Eng J* 174:117–125
- 657 18. Kecira Z, Benturki O, Benturki A, et al (2020) High adsorption capacity of nitrobenzene from
658 aqueous solution using activated carbons prepared from vegetable waste. *Environ Prog*
659 *Sustain Energy* 39:e13463
- 660 19. Mokhati A, Benturki O, Benturki A, et al (2022) Conversion of Argan Nutshells into Novel
661 Porous Carbons in the Scope of Circular Economy: Adsorption Performance of Emerging
662 Contaminants. *Appl Sci* 12:. <https://doi.org/10.3390/app12157607>
- 663 20. Zhou J, Luo A, Zhao Y (2018) Preparation and characterisation of activated carbon from waste
664 tea by physical activation using steam. *J Air Waste Manage Assoc* 68:1269–1277
- 665 21. Pallarés J, González-Cencerrado A, Arauzo I (2018) Production and characterization of
666 activated carbon from barley straw by physical activation with carbon dioxide and steam.
667 *Biomass and Bioenergy* 115:64–73
- 668 22. Muniandy L, Adam F, Mohamed AR, Ng E-P (2014) The synthesis and characterization of high
669 purity mixed microporous/mesoporous activated carbon from rice husk using chemical
670 activation with NaOH and KOH. *Microporous Mesoporous Mater* 197:316–323
- 671 23. Kumar A, Jena HM (2017) Adsorption of Cr (VI) from aqueous solution by prepared high
672 surface area activated carbon from Fox nutshell by chemical activation with H₃PO₄. *J Environ*
673 *Chem Eng* 5:2032–2041
- 674 24. Chen Y-D, Chen W-Q, Huang B, Huang M-J (2013) Process optimization of K₂C₂O₄-activated
675 carbon from kenaf core using Box–Behnken design. *Chem Eng Res Des* 91:1783–1789
- 676 25. Mai NT, Nguyen MN, Tsubota T, et al (2021) Evolution of physico-chemical properties of
677 *Dicranopteris linearis*-derived activated carbon under various physical activation
678 atmospheres. *Sci Rep* 11:1–9
- 679 26. Laginhas C, Nabais JMV, Titirici MM (2016) Activated carbons with high nitrogen content by a
680 combination of hydrothermal carbonization with activation. *Microporous Mesoporous Mater*
681 226:125–132
- 682 27. Daoud M, Benturki O, Kecira Z, et al (2017) Removal of reactive dye (BEZAKTIV Red S-MAX)
683 from aqueous solution by adsorption onto activated carbons prepared from date palm rachis
684 and jujube stones. *J Mol Liq* 243:. <https://doi.org/10.1016/j.molliq.2017.08.093>
- 685 28. Daoud M, Benturki O, Girods P, et al (2019) Adsorption ability of activated carbons from
686 *Phoenix dactylifera* rachis and *Ziziphus jujube* stones for the removal of commercial dye and
687 the treatment of dyestuff wastewater. *Microchem J* 148:.
688 <https://doi.org/10.1016/j.microc.2019.05.022>
- 689 29. Daoud M, Benturki O, Fontana S, et al (2019) Energy and matter balance of process of
690 activated carbon production from Algerian agricultural wastes: date palm rachis and jujube
691 stones. *Biomass Convers Biorefinery*. <https://doi.org/10.1007/s13399-019-00543-w>
- 692 30. Daoud M, Benturki O, Kecira Z, et al (2022) The effect of steam on the physicochemical
693 properties of activated carbons based on *Ziziphus jujube* stones for reactive dye removal.

- 694 Biomass Convers Biorefinery 1–14
- 695 31. Burg P, Vix-Guterl C (2005) Importance de la chimie de surface des matériaux carbonés. *Actual*
696 *Chim* 91–94
- 697 32. Figueiredo JL, Pereira MFR, Freitas MMA, Orfao JJM (1999) Modification of the surface
698 chemistry of activated carbons. *Carbon N Y* 37:1379–1389
- 699 33. Contescu A, Contescu C, Putyera K, Schwarz JA (1997) Surface acidity of carbons characterized
700 by their continuous pK distribution and Boehm titration. *Carbon N Y* 35:83–94
- 701 34. de Souza TNV, de Carvalho SML, Vieira MGA, et al (2018) Adsorption of basic dyes onto
702 activated carbon: experimental and theoretical investigation of chemical reactivity of basic
703 dyes using DFT-based descriptors. *Appl Surf Sci* 448:662–670
- 704 35. Van Tran T, Nguyen H, Le PHA, et al (2020) Microwave-assisted solvothermal fabrication of
705 hybrid zeolitic–imidazolate framework (ZIF-8) for optimizing dyes adsorption efficiency using
706 response surface methodology. *J Environ Chem Eng* 8:104189
- 707 36. Rocha LS, Sousa ÉML, Gil M V, et al (2021) Producing magnetic nanocomposites from paper
708 sludge for the adsorptive removal of pharmaceuticals from water—a fractional factorial
709 design. *Nanomaterials* 11:287
- 710 37. Egbosiuba TC, Abdulkareem AS, Tijani JO, et al (2021) Taguchi optimization design of
711 diameter-controlled synthesis of multi walled carbon nanotubes for the adsorption of Pb (II)
712 and Ni (II) from chemical industry wastewater. *Chemosphere* 266:128937
- 713 38. de Luna MDG, Sablas MM, Hung C-M, et al (2020) Modeling and optimization of imidacloprid
714 degradation by catalytic percarbonate oxidation using artificial neural network and Box-
715 Behnken experimental design. *Chemosphere* 251:126254
- 716 39. Chaker H, Ameer N, Saidi-Bendahou K, et al (2021) Modeling and Box-Behnken design
717 optimization of photocatalytic parameters for efficient removal of dye by lanthanum-doped
718 mesoporous TiO₂. *J Environ Chem Eng* 9:104584
- 719 40. Yasir M, Chauhan I, Zafar A, et al (2021) Buspirone loaded solid lipid nanoparticles for
720 amplification of nose to brain efficacy: Formulation development, optimization by Box-
721 Behnken design, in-vitro characterization and in-vivo biological evaluation. *J Drug Deliv Sci*
722 *Technol* 61:102164
- 723 41. Zhang Y-J, Xing Z-J, Duan Z-K, et al (2014) Effects of steam activation on the pore structure and
724 surface chemistry of activated carbon derived from bamboo waste. *Appl Surf Sci* 315:279–
725 286. <https://doi.org/https://doi.org/10.1016/j.apsusc.2014.07.126>
- 726 42. Gonzalez JF, Roman S, González-García CM, et al (2009) Porosity development in activated
727 carbons prepared from walnut shells by carbon dioxide or steam activation. *Ind Eng Chem Res*
728 48:7474–7481
- 729 43. Jagiello J, Kenvin J, Celzard A, Fierro V (2019) Enhanced resolution of ultra micropore size
730 determination of biochars and activated carbons by dual gas analysis using N₂ and CO₂ with
731 2D-NLDFT adsorption models. *Carbon N Y* 144:206–215
- 732 44. Zhang T, Walawender WP, Fan LT, et al (2004) Preparation of activated carbon from forest
733 and agricultural residues through CO₂ activation. *Chem Eng J* 105:53–59
- 734 45. Juang R-S, Wu F-C, Tseng R-L (2002) Characterization and use of activated carbons prepared
735 from bagasses for liquid-phase adsorption. *Colloids Surfaces A Physicochem Eng Asp* 201:191–
736 199

- 737 46. Sidi-Yacoub B, Oudghiri F, Belkadi M, Rodríguez-Barroso R (2019) Characterization of
738 lignocellulosic components in exhausted sugar beet pulp waste by TG/FTIR analysis. *J Therm*
739 *Anal Calorim* 138:1801–1809
- 740 47. Dittmann D, Saal L, Zietzschmann F, et al (2022) Characterization of activated carbons for
741 water treatment using TGA-FTIR for analysis of oxygen-containing functional groups. *Appl*
742 *Water Sci* 12:203. <https://doi.org/10.1007/s13201-022-01723-2>
- 743 48. Jawad AH, Abdulhameed AS, Wilson LD, et al (2021) High surface area and mesoporous
744 activated carbon from KOH-activated dragon fruit peels for methylene blue dye adsorption:
745 Optimization and mechanism study. *Chinese J Chem Eng* 32:281–290
- 746 49. Mritunjay, Quaff AR (2022) Adsorption of copper on activated Ganga sand from aqueous
747 solution: kinetics, isotherm, and optimization. *Int J Environ Sci Technol* 19:9679–9690.
748 <https://doi.org/10.1007/s13762-021-03651-1>
- 749 50. Kumar S, Quaff AR (2020) Treatment of domestic wastewater containing phosphate using
750 water treatment sludge through UASB–clariflocculator integrated system. *Environ Dev Sustain*
751 *22:4537–4550*
- 752 51. Nair AT, Makwana AR, Ahammed MM (2014) The use of response surface methodology for
753 modelling and analysis of water and wastewater treatment processes: a review. *Water Sci*
754 *Technol* 69:464–478
- 755 52. Kuang Y, Zhang X, Zhou S (2020) Adsorption of methylene blue in water onto activated carbon
756 by surfactant modification. *Water* 12:587
- 757 53. Nayak AK, Pal A (2019) Development and validation of an adsorption kinetic model at solid-
758 liquid interface using normalized Gudermannian function. *J Mol Liq* 276:67–77
- 759 54. Ojedokun AT, Bello OS (2017) Liquid phase adsorption of Congo red dye on functionalized
760 corn cobs. *J Dispers Sci Technol* 38:1285–1294
- 761 55. Ghibate R, Senhaji O, Taouil R (2021) Kinetic and thermodynamic approaches on Rhodamine B
762 adsorption onto pomegranate peel. *Case Stud Chem Environ Eng* 3:100078
- 763 56. Malhotra M, Suresh S, Garg A (2018) Tea waste derived activated carbon for the adsorption of
764 sodium diclofenac from wastewater: adsorbent characteristics, adsorption isotherms, kinetics,
765 and thermodynamics. *Environ Sci Pollut Res* 25:32210–32220
- 766 57. Pirbazari AE, Saberikhah E, Badrouh M, Emami MS (2014) Alkali treated Foumanat tea waste
767 as an efficient adsorbent for methylene blue adsorption from aqueous solution. *Water Resour*
768 *Ind* 6:64–80
- 769 58. Abdel-Gawad SA, Abdel-Aziz HM (2019) Removal of ethinylestradiol by adsorption process
770 from aqueous solutions using entrapped activated carbon in alginate biopolymer: isotherm
771 and statistical studies. *Appl Water Sci* 9:75. <https://doi.org/10.1007/s13201-019-0951-7>
- 772 59. Benderdouche N, Bestani B, Hamzaoui M (2018) The use of linear and nonlinear methods for
773 adsorption isotherm optimization of basic green 4-dye onto sawdust-based activated carbon.
774 *J Mater Environ Sci* 9:1110–1118
- 775 60. Wang H, Li Z, Yahyaoui S, et al (2021) Effective adsorption of dyes on an activated carbon
776 prepared from carboxymethyl cellulose: Experiments, characterization and advanced
777 modelling. *Chem Eng J* 417:128116
- 778 61. Jain SN, Tamboli SR, Sutar DS, et al (2020) Incense stick ash as a novel and sustainable
779 adsorbent for sequestration of Victoria Blue from aqueous phase. *Sustain Chem Pharm*

- 780 15:100199
- 781 62. Nasrullah A, Saad B, Bhat AH, et al (2019) Mangosteen peel waste as a sustainable precursor
782 for high surface area mesoporous activated carbon: Characterization and application for
783 methylene blue removal. *J Clean Prod* 211:1190–1200.
784 <https://doi.org/https://doi.org/10.1016/j.jclepro.2018.11.094>
- 785 63. Liu T, Li Y, Du Q, et al (2012) Adsorption of methylene blue from aqueous solution by
786 graphene. *Colloids Surfaces B Biointerfaces* 90:197–203
- 787 64. Durrani WZ, Nasrullah A, Khan AS, et al (2022) Adsorption efficiency of date palm based
788 activated carbon-alginate membrane for methylene blue. *Chemosphere* 302:134793
- 789 65. Altalhi TA, Ibrahim MM, Mersal GAM, et al (2022) Adsorption of doxorubicin hydrochloride
790 onto thermally treated green adsorbent: Equilibrium, kinetic and thermodynamic studies. *J*
791 *Mol Struct* 1263:133160
- 792 66. Márquez P, Benítez A, Chica AF, et al (2022) Evaluating the thermal regeneration process of
793 massively generated granular activated carbons for their reuse in wastewater treatments
794 plants. *J Clean Prod* 366:132685
- 795